scientific reports

Check for updates

OPEN

Importance of residue 248 in *Escherichia coli* RNase P RNA mediated cleavage

Guanzhong Mao[1], Abhishek S. Srivastava[1,2], Shiying Wu[1,2], David Kosek[1] & Leif A. Kirsebom[1]✉

tRNA genes are transcribed as precursors and RNase P generates the matured 5′ end of tRNAs. It has been suggested that residue −1 (the residue immediately 5′ of the scissile bond) in the pre-tRNA interacts with the well-conserved bacterial RNase P RNA (RPR) residue A_{248} (*Escherichia coli* numbering). The way A_{248} interacts with residue −1 is not clear. To gain insight into the role of A_{248}, we analyzed cleavage as a function of A_{248} substitutions and N_{-1} nucleobase identity by using pre-tRNA and three model substrates. Our findings are consistent with a model where the structural topology of the active site varies and depends on the identity of the nucleobases at, and in proximity to, the cleavage site and their potential to interact. This leads to positioning of Mg^{2+} that activates the water that acts as the nucleophile resulting in efficient and correct cleavage. We propose that in addition to be involved in anchoring the substrate the role of A_{248} is to exclude bulk water from access to the amino acid acceptor stem, thereby preventing non-specific hydrolysis of the pre-tRNA. Finally, base stacking is discussed as a way to protect functionally important base-pairing interactions from non-specific hydrolysis, thereby ensuring high fidelity during RNA processing and the decoding of mRNA.

The tRNA genes are transcribed as precursors (pre-tRNA) and several enzymes are involved in the processing of pre-tRNA. Among these endoribonuclease P (RNase P) is responsible for generating tRNAs with matured 5′ ends. RNase P from all three kingdoms of life consists of both RNA and protein; in Bacteria, RNase P is composed of one RNA (RPR) and one protein subunit, C5. Irrespective of origin, the catalytic activity was thought to reside in the RPR[1,2]. Recent data, however, show that there exist RNase P activities solely based on proteins, (referred to as PRORPs) in human mitochondria, *Arabidopsis thaliana*, *Trypanosoma brucei*, in the algae *Ostreococcus tauri* and in *Aquifex aeolicus*[3–7].

At high ionic strength, RPRs of different origins cleave pre-tRNA and a number of non-tRNA substrates efficiently at the correct site without proteins[1,8–12]. The RPR interacts with several regions of pre-tRNAs and model substrates. These are: the 3′ terminal RCC-motif (the RCCA-RNase P interaction, interacting residues underlined)[13]; and the T-stem/loop- (TSL) region of pre-tRNAs binds to the RPR TSL-binding site or TBS in the specificity (S) domain. In addition, the residue immediately 5′ of the cleavage site (N_{-1}) is in close proximity to A_{248} (referred to as the A_{248}/N_{-1} interaction and *Escherichia coli* numbering; Fig. 1). The crystal structure of bacterial (*Thermotoga maritima*) RNase P in complex with tRNA and recent cryo-EM structures of yeast, archaeal and human RNase P in complex with pre-tRNA (yeast) and tRNA suggest that in particular the TSL–TBS interaction is evolutionary conserved[11,14–21], (see also[22]).

Residue A_{248} is well-conserved among bacterial RPRs. However, the nature of the A_{248}/N_{-1} interaction is less clear. In the bacterial RNase P-tRNA co-crystal structure A_{248} is positioned close to the tRNA 5′ end[18]. This is also observed in the cryo-EM structure of an archaeal RNase P in complex with tRNA[20]. On the basis of biochemical and genetic data using *E. coli* (*Eco*) RPR, A_{248} has been proposed to form a *cis* Watson–Crick/Watson–Crick (*cis* WC/WC)[23] pair with the N_{-1} residue in the substrate[24,25]. The identity of residue −1 in pre-tRNAs varies in *E. coli* and other bacteria, but in many of them it is a uridine[26–28]. We have provided data that this pairing does not correspond to a standard Watson–Crick pairing. Rather, the N_{-1} residue binds to a pocket where $A_{248(wt)}$ plays a central role, but it does not directly pair with the −1 residue[16,29–31]. Nucleotide analogue-modification interference studies further suggest that the Hoogsteen surface of A_{248} is important for a productive interaction with the substrate[32]. However, kinetic data argue against that N7 and $6NH_2$ of A_{248} form hydrogen bonds with the 2′OH and O2 (when present on the nucleobase, i.e. C or U) of residue −1, respectively, which both are oriented in the same direction in a structural model of the cleavage site[31]. Thus, the function of A_{248}—and whether it interacts

[1]Department of Cell and Molecular Biology, Biomedical Centre, Box 596, 751 24 Uppsala, Sweden. [2]These authors contributed equally: Abhishek S. Srivastava and Shiying Wu. ✉email: Leif.Kirsebom@icm.uu.se

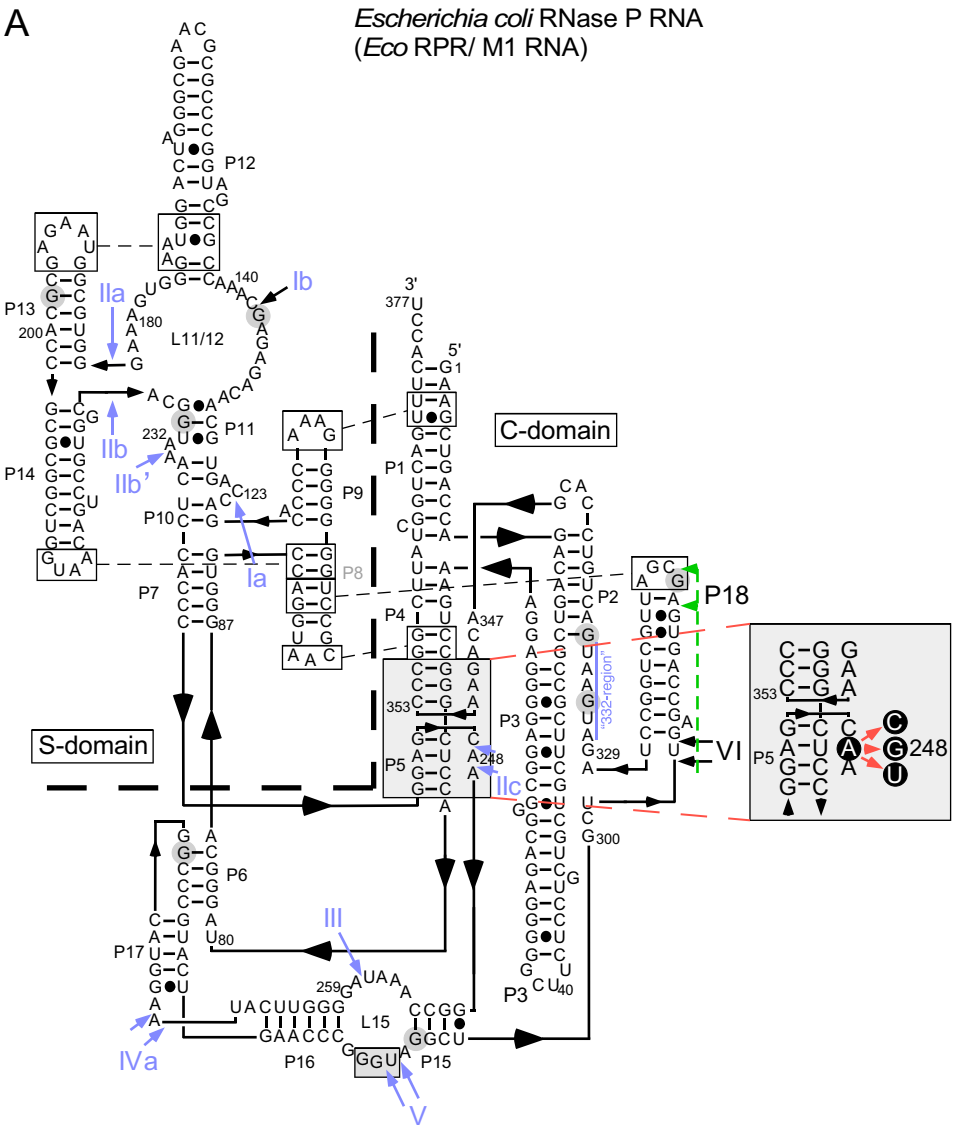

Figure 1. Illustration of the *Eco* RPR secondary structures. (**A**) *Eco* RPR secondary structure according to Massire et al.[90]. The heavy dashed demarcation line separates the S- and C-domains. The large gray box highlights the A_{248}-region, and show the substitutions that were introduced at 248 (red arrows). The gray box in L15 marks residues that pair with the substrate 3′ end—the RCCA-RNase P RNA interaction (interacting residues underlined)[12]—in the RPR-substrate complex. The blue arrows and Roman numerals mark the Pb^{2+}-induced cleavage sites as shown in Fig. 2 (black circles). The vertical line marked in blue marks the "332-region", which is also cleaved in the in presence of Pb^{2+}(see also[85,91]). Residues highlighted with gray circles correspond to RNase T1 cleavage sites (see also Fig. 2, bands marked with red dots)[92]. The green dashed line and arrows mark the area in P18, which becomes accessible to RNase T1 cleavage upon on substitution of A_{248} with U (see Fig. 2, *Eco* RPR_{U248}). (**B**) Sequence of alignment of the region which includes the conserved *E. coli* (Ec) A_{248}, *T. maritima* (Tm[93]) A_{213}, *M. tuberculosis* (Mtb[28]) A_{248} and the Archaea *P. furiosus* (Pfu[9,12]) A_{218}, and neighboring sequences as indicated.

with residue −1—remains unclear. The crystal and cryo-EM structures of the RNase P-tRNA complexes (bacteria and archaea) do not provide guidance because these structures represent the post cleavage stage of the RNase P catalyzed reaction[18,20]. We therefore decided to revisit and investigate the interrelationship between residue −1 and A_{248}. To achieve this, we studied cleavage of all ribo pre-tRNA and model hairpin loop substrates, carrying different nucleobases at position −1 with *Eco* RPR 248-variants.

Here we provide data that the identities of both residue N_{-1} in the substrate and residue 248 in the RPR influence cleavage site selection and rate of cleavage. However, our data do not support the model where the well-conserved residue $A_{248(wt)}$ forms a *cis* WC/WC pair with N_{-1}. This was particularly apparent studying different substrates carrying 3-methyl U at the N_{-1} position. Our combined data support a model where the structural topology of the active site varies and depends on the identity of the nucleobases at, and in proximity to, the cleavage site and their potential to interact. As a consequence, this affects the positioning of Mg^{2+} that activates the water that acts as the nucleophile resulting in efficient and correct cleavage. In this scenario we suggest that, besides participating in the anchoring of the substrate, the role of A_{248} in wild type bacterial RPR, which stacks on the tRNA G_{+1}/C_{+72} base pair, is to exclude bulk water from accessing the amino acid acceptor stem and thereby prevent non-specific hydrolysis/cleavage of the pre-tRNA.

Results

Substituting residue 248 has minor effects on the overall structure of Eco RPR. To investigate the role and contribution of the well-conserved A_{248} to *Eco* RPR mediated cleavage we used wild type *Eco* $RPR_{A248(wt)}$ and three 248 variants: *Eco* RPR_{C248}, *Eco* RPR_{G248} and *Eco* RPR_{U248} (Fig. 1). The generation and catalytic performance of *Eco* RPR_{G248} has been reported elsewhere[30,31], while the other two RPRs were generated as outlined in "Materials and methods". As predicted on the basis of previous studies, the C_{248} and U_{248} variants were catalytically active[24] (see below).

First, we inquired whether substitution of $A_{248(wt)}$ with any of the other nucleobases affected the structure of *Eco* RPR. On the basis of structural probing with Pb^{2+} and RNase T1 (which cleaves 3′ of single stranded G residues) we reported that the overall structures of *Eco* $RPR_{A248(wt)}$ and *Eco* RPR_{G248} are very similar[31]. This was also the case for the C_{248} variant [Fig. 2; cf. lanes 2 and 3 (*Eco* $RPR_{A248(wt)}$) and lanes 11 and 12 (*Eco* RPR_{C248})]. By contrast, a U at 248 affected the structure such that G-residues between P15 and the P18-loop became accessible to RNase T1 [Fig. 1; cf. lanes 3 (*Eco* $RPR_{A248(wt)}$) and 6 (*Eco* RPR_{U248})]. This suggested that a U at 248 influences the structural integrity of P18, which plays a role in connecting the C- and S-domain via the P8/P18-interaction (Fig. 1). Moreover, compared to *Eco* $RPR_{A248(wt)}$, exposure to RNase T1 resulted in the appearance of an additional weak cleavage product located between residues 276 and 292, in particular in the case of G_{248} (Fig. 2; bands marked with *). This might indicate a change in the structure in this region in response to mutating $A_{248(wt)}$, see also Ref.[31]. With respect to the Pb^{2+}-induced cleavage patterns, we did not detect any apparent difference comparing the 248 variants [Fig. 2; cf. lanes 2 ($A_{248(wt)}$), 5 (U_{248}), 8 (C_{248}) and 11 (G_{248})]. We conclude that substitution of A_{248} in wild type *Eco* RPR resulted in a small (if any) overall structural effect with the exception of U_{248} where a notable structural change was detected in P18.

Catalytic performance as a function of replacing the well-conserved A_{248} in *Eco* RPR. *Choice of substrates and experimental outline.* The role of residues A_{248} in *Eco* $RPR_{A248(wt)}$ and −1 in the substrate has previously been analyzed using variants of a *Bacillus subtilis* $tRNA^{Asp}$ precursor[24,25]. From these studies, the authors proposed a model where the −1 residue in the substrate forms a *cis* Watson–Crick (WC) base pair with A_{248}. The model predicts that (i) breakage of this interaction shifts cleavage from the correct to an alternative site (see below), and (ii) introduction of a compensatory change that restores the N_{-1}/N_{248} pairing should increase (rescue) cleavage at the correct site. To test this model and to investigate the role of A_{248}, we used N_{-1} derivatives of the *E. coli* $tRNA^{Ser}$Su1 precursor, pSu1[13,33], and two well-characterized model hairpin loop substrates, pATSer and pMini3bp, both derived from pSu1 (Fig. 3)[15,31,34–36]. The pATSer substrates have the amino acceptor-stem and T-stem intact while pMini3bp lacks the T-stem, T-loop and part of the acceptor-stem. Two pATSer variants were used, the first has the original T-loop (e.g. pATSerUG where U and G correspond to the residues at −1 and "+73", respectively; numbering refers to the position in tRNA; Fig. 3). In the other, the T-loop is substituted with a GAAA-tetra loop (e.g. $pATSerUG_{GAAA}$). The latter interacts differently with *Eco* $RPR_{A248(wt)}$; it increases cleavage at the alternative site between −2 and −1 (Fig. 3C; see below)[15,30,37]. The short model substrates pMini3bp all have three-base-pair short stems, capped with GAAA-tetra loops (e.g. pMini3bpUG). Importantly, pSu1 and pATSer can interact with the TBS-region (see above) upon *Eco* RPR substrate complex formation, while pATSer variants with GAAA-tetra loops and pMini3bp cannot (or interact differently) due to their sizes and/or the presence of the GAAA-tetra loop[15,30,31,38]. We introduced the natural ribonucleobases (A, C, G and U) at position −1 (N_{-1}) in all four substrate variants. For pATSer and pMini3bp, we also used variants carrying chemically modified ribonucleobases at −1 and +73. Varying both residue −1 and +73 allowed us to investigate the importance of having nucleobases at −1 that can pair with residue +73 with different numbers of hydrogen bonds. To further investigate whether U_{-1} in the model substrates pairs with $A_{248(wt)}$ in *Eco* RPR we introduced a methyl group (**3mU**) at −1 (Fig. 3E), which interferes with *cis* WC/WC pairing with $A_{248(wt)}$. Finally, we replaced the 2′OH with $2'NH_2$ (or 2′H) and varied the +1/+72 base pair in pATSerUG to probe the de-protonation of the $2'NH_2$ (charge distribution; see below) at the canonical cleavage site in the RPR-substrate complex as a function of N_{248} identity (Fig. 3)[38–40].

The Mg^{2+} concentration for optimal cleavage rates of pMini3bp substrates using *Eco* $RPR_{A248(wt)}$ and *Eco* RPR_{G248} is 800 mM; this is higher than for the other substrates[15,30,31]. Moreover, on the basis of our published data where we studied cleavage of pATSer and pMini3bp variants using *Eco* $RPR_{A248(wt)}$ and *Eco* RPR_{G248}, we assumed that optimal cleavage rates are reached at 800 mM Mg^{2+} also for the other 248 variants[15,30,31,37]. To be

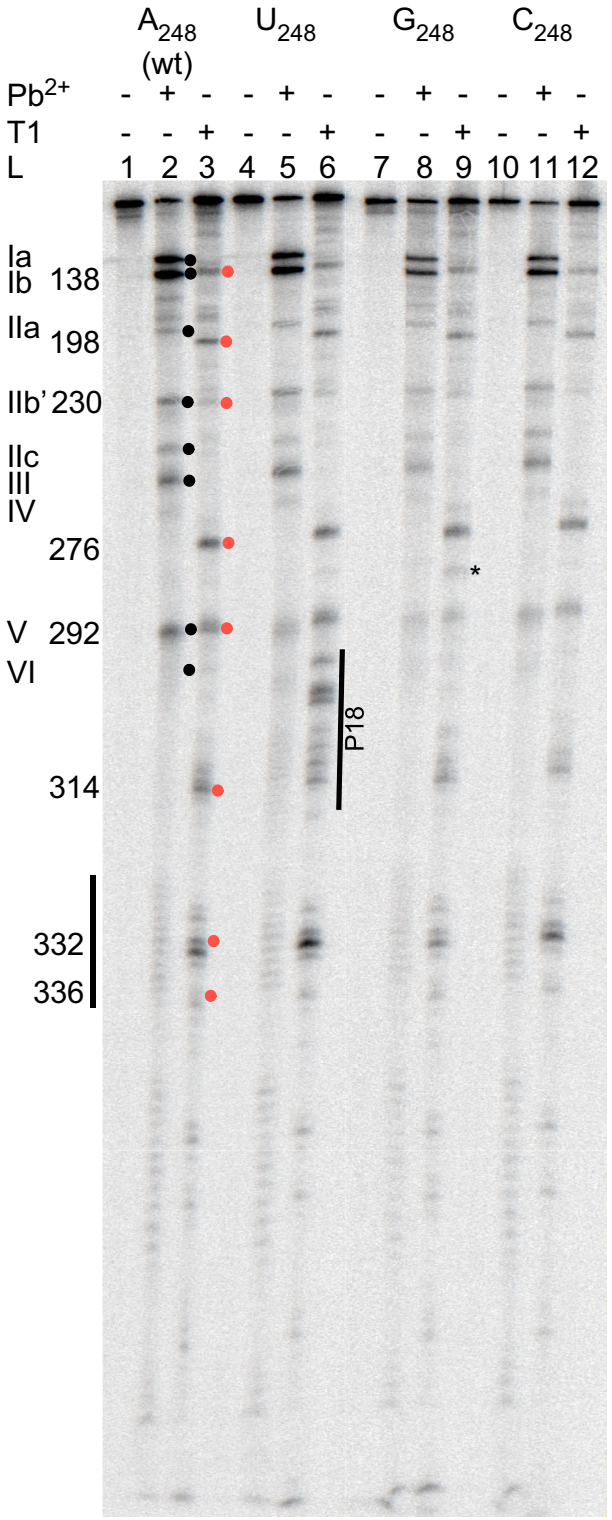

Figure 2. Structural probing of *Eco* RPR. Probing the structures of the *Eco* RPR 248-variants with Pb^{2+} and RNase T1. Roman numerals and black circles refer to Pb^{2+}-induced cleavage sites in *Eco* RPR (Fig. 1)[31,85,91]. Numbers and red circles correspond to the RNase T1 cleavage sites according to Guerrier-Takada and Altman[92], see Fig. 1A. The vertical black lines mark the P18- and 332-region. The vertical black line "P18" marks the extra RNase T1 cleavage sites between 292 and 314 in the U_{248} variant. The reactions were conducted using 0.5 mM $Pb(OAc)_2$ and RNase T1 as described in "Materials and methods".

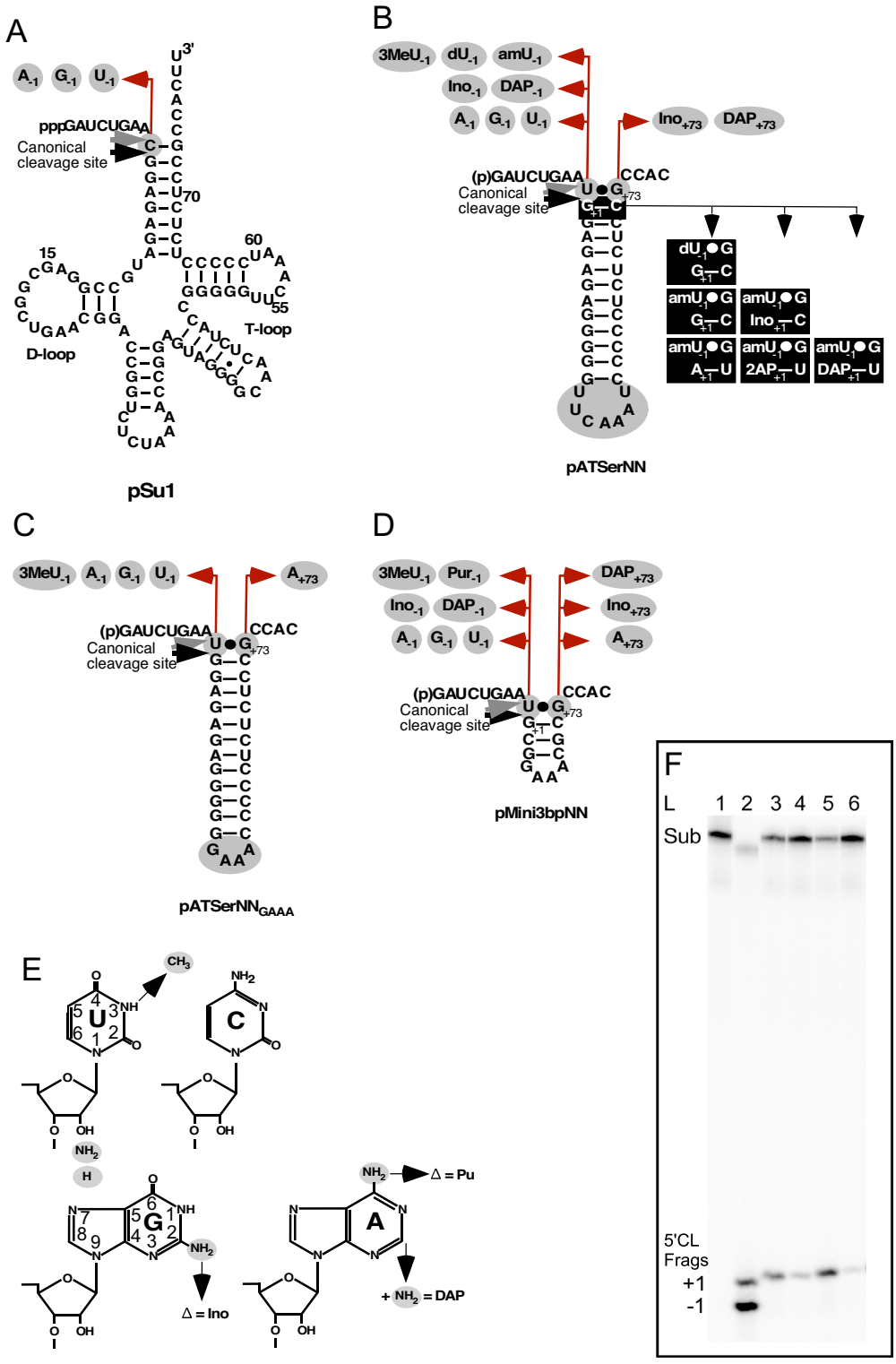

Figure 3. Secondary structure of substrates used in the present study. (**A**) pSu1, (**B**) pATSerNN, (**C**) pATSerNN$_{GAAA}$, (**D**) pMini3bp, (**E**) structures of nucleobases, and (**F**) cleavage of pATSerUG by the different *Eco* RPR 248 variants. Residues highlighted in gray were introduced to generate the different variants carrying alternative nucleobases at positions −1 and +73. The black boxes illustrate the changes that generated substrates carrying 2′NH$_2$ and 2′H as well as substitutions of residues at positions +1 and +72. The canonical (correct) cleavage sites between residues N$_{-1}$ and N$_{+1}$ in the different substrates are marked with black arrows. The gray arrows mark the alternative cleavage sites between N$_{-2}$ and N$_{-1}$ (referred to as position −1, see text). The seven-base loop (**B**, marked in gray) in pATSerNN was replaced with a GAAA-tetra loop (**C**, marked in gray) to generate pATSerNN$_{GAAA}$, see[14,15]. Panel (**F**): lane (L) 1, pATSerUG no RPR added; lane 2, cleavage of pATSerCG$_{GAAA}$ with *Eco* RPR$_{A248(wt)}$; lane 3, cleavage of pATSerUG with *Eco* RPR$_{A248(wt)}$; lane 4, cleavage of pATSerUG with *Eco* RPR$_{C248}$; lane 5, cleavage of pATSerUG with *Eco* RPR$_{G248}$; lane 6, cleavage of pATSerUG with *Eco* RPR$_{U248}$. Sub, substrate and 5′CL Frags marks the migration of the 5′ cleavage products as a result of cleavage at +1 and −1. The reaction was performed in buffer C at 800 mM Mg^{2+} with 0.8 µM *Eco* RPR (irrespective of variant) and ≤ 0.02 µM substrate for 10 s as described in "Materials and methods".

able to directly compare the cleavage rates, we decided to perform all the experiments discussed below at 800 mM Mg^{2+}. Also, at this Mg^{2+} concentration the likelihood of detecting cleavage increases, see e.g.,[31]. We emphasize that the C5 protein interacts with residues N_{-4}–N_{-8} in the 5′ leader but not N_{-1}[41,42] and that we were primarily interested in the catalytic performance of the RPR in the absence of C5. Hence, these studies were performed without the C5 protein.

Cleavage of the different substrates was studied with respect to (i) cleavage site recognition and (ii) rate of cleavage (single turnover; see "Materials and methods"). The canonical (also referred to as correct cleavage or the +1 position) site corresponds to cleavage between residues −1 and +1 (Fig. 3), while cleavage at other positions are referred to as alternative sites or miscleavage; e.g., cleavage at −1 relates to cleavage between −2 and −1 in the 5′ leader. The frequencies of cleavage at +1 are presented in Figs. 4, 6 and 8 while the rate constants (k_{app}), determined under single turnover conditions for the combinations discussed above, are shown in Tables 1, 2

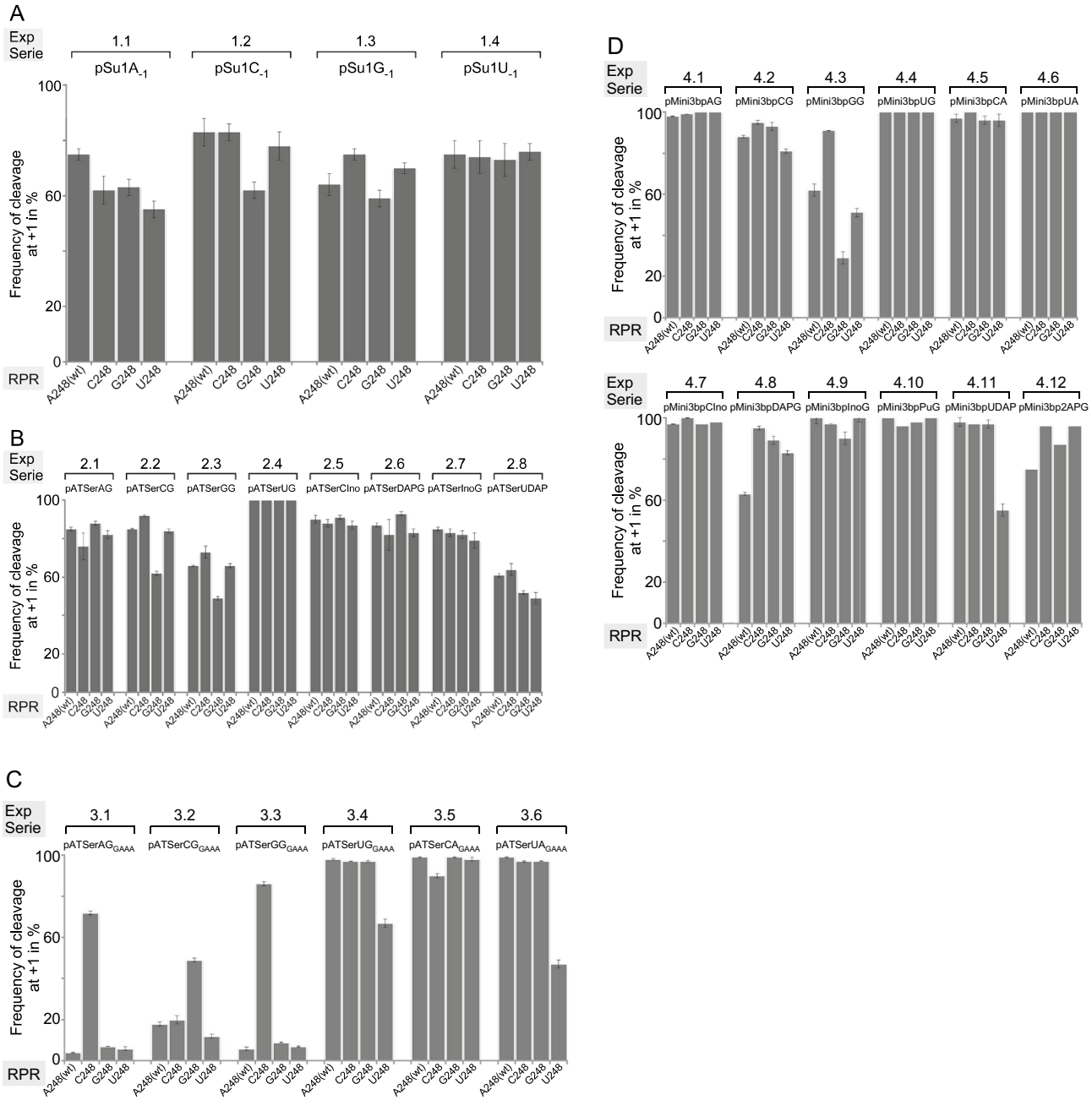

Figure 4. Frequencies of cleavage at +1 by *Eco* RPR 248 variants. Histograms summarizing frequencies of cleavage at +1 in % for the various substrate and *Eco* RPR 248 combinations as indicated. (**A**) Cleavage of pSu1(N_{-1}) variants, Exp Series (ExpS) 1.1–1.4. (**B**) Cleavage of pATSer($N_{-1}N_{+73}$) variants, Exp Series (ExpS) 2.1–2.8. (**C**) Cleavage of pATSer$(N_{-1}N_{+73})_{GAAA}$ variants, Exp Series (ExpS) 3.1–3.6. (**D**) Cleavage of pMini3bpN_{-1}/N_{+73} variants, Exp Series (ExpS) 4.1–4.12. To calculate the frequencies of cleavage at +1 we used the 5′ cleavage fragments and mean and experimental errors were calculated from at least three independent experiments.

	ExpS	CL Site	A_{248} wt	RPR variant		
				C_{248}	G_{248}	U_{248}
$pSu1A_{-1}$	1.1	+1	47 ± 3	32 ± 1	58 ± 5	38 ± 7
		−1	3.5 ± 0.6	3 ± 0.4	4 ± 0.5	8 ± 0.7
$pSu1C_{-1}$	1.2	+1	71 ± 7	44 ± 5	43 ± 4	46 ± 3
		−1	5 ± 0.1	2.5 ± 0.2	17 ± 1	5 ± 1
$pSu1G_{-1}$	1.3	+1	41 ± 2	44 ± 4	39 ± 0.7	36 ± 4
		−1	6 ± 0.6	2 ± 0.2	12 ± 1	4 ± 0.3
$pSu1U_{-1}$	1.4	+1	**121 ± 4**	70 ± 3	85 ± 3	47 ± 3
		−1	4 ± 0.4	3 ± 0.1	4 ± 0.5	3 ± 0.3
pATSerAG	2.1	+1	64 ± 6.9	4.3 ± 0.2	**90 ± 6.4**	36 ± 3.4
		−1	8 ± 2	0.8 ± 0.1	10 ± 1	6 ± 0.8
pATSerCG	2.2	+1	51 ± 1.2	10 ± 0.2	11 ± 0.5	24 ± 0.5
		−1	9 ± 0.7	0.9 ± 0.1	7 ± 0.5	4 ± 0.2
pATSerGG	2.3	+1	40 ± 4.4	26 ± 1	48 ± 2.5	28 ± 6
		−1	15 ± 3	7 ± 0.5	41 ± 2	11 ± 2
pATSerUG	2.4	+1	73 ± 1	32 ± 3	61 ± 0.4	11 ± 0.2
		−1	ND	ND	ND	ND
pATSerCIno	2.5	+1	47 ± 5	17 ± 2.2	61 ± 11	19 ± 0.1
		−1	4 ± 0.4	2 ± 0.4	5 ± 1	2 ± 0.1
pATSerDAPG	2.6	+1	47 ± 1	4 ± 1	72 ± 3.4	19 ± 0.5
		−1	6 ± 0.8	0.5 ± 0.02	4 ± 0.2	2 ± 0.1
pATSerInoG	2.7	+1	**89 ± 2.7**	53 ± 3.2	63 ± 3.2	30 ± 2.6
		−1	11 ± 1	8 ± 2	9 ± 1	6 ± 0.5
pATSerUDAP	2.8	+1	46 ± 1.2	16 ± 0.47	37 ± 2.7	8 ± 0.55
		−1	22 ± 1	7 ± 0.1	25 ± 1	6 ± 0.5
$pATSerAG_{GAAA}$	3.1	+1	0.3 ± 0.01	0.4 ± 0.05	0.6 ± 0.05	0.07 ± 0.01
		−1	6 ± 0.2	0.09 ± 0.01	7.3 ± 0.7	0.7 ± 0.1
$pATSerCG_{GAAA}$	3.2	+1	0.8 ± 0.05	0.01 ± 0.002	5 ± 0.6	0.07 ± 0.004
		−1	2.4 ± 0.2	0.05 ± 0.007	5 ± 0.5	0.8 ± 0.08
$pATSerGG_{GAAA}$	3.3	+1	0.4 ± 0.06	0.46 ± 0.01	0.55 ± 0.1	0.04 ± 0.003
		−1	7 ± 1	0.06 ± 0.001	5.5 ± 0.7	0.54 ± 0.04
$pATSerUG_{GAAA}$	3.4	+1	22 ± 2	0.6 ± 0.05	13 ± 1	0.04 ± 0.006
		−1	0.4 ± 0.005	0.03 ± 0.002	0.4 ± 0.01	0.01 ± 0.002
$pATSerCA_{GAAA}$	3.5	+1	9 ± 0.8	0.14 ± 0.01	**26 ± 4**	1 ± 0.1
		−1	0.1 ± 0.03	$0.02 \pm 1 \times 10^{-4}$	ND	0.04 ± 0.002
$pATSerUA_{GAAA}$	3.6	+1	10 ± 0.8	0.14 ± 0.01	3 ± 0.4	0.01 ± 0.002
		−1	0.1 ± 0.01	$0.02 \pm 1 \times 10^{-4}$	0.07 ± 0.01	0.01 ± 0.002

Table 1. Rate of cleavage (k_{app}) for pSu1, pATSer and $pATSer_{GAAA}$ derivatives using different RPR variants without the C5 protein. The data represent mean ± experimental errors calculated from at least three independent experiments and are expressed as cleavage per min per pmol of RPR. Dependent on RPR substrate combination, between 0.4 and 0.8 µM RPR was used, and 2 nM of substrate in all cases. The reactions were performed at 37 °C in buffer C at 800 mM Mg^{2+} (see "Materials and methods") and the "substrate-N_{248}" combinations showing the highest rates are highlighted in bold.

and 3. For clarity and guidance, the experiments using different substrate/RPR (N_{248}) combinations are referred to as "Experiment Series (ExpS)" in the figures and tables where 1.1 corresponds to substrate 1, pSu1, having A at −1 while 1.2 has C, i.e. $pSu1A_{-1}$ and $pSu1C_{-1}$, respectively, and substrate 2.1 pATSer having A_{-1} and G_{+73} (pATSerAG and A_{-1}/G_{+73} substrate/variant) etc. In the first set of experiments we studied cleavage of the full-size pre-$tRNA^{Ser}$Su1 (pSu1; ExpS 1.1–1.4) and pATSer N_{-1}/N_{+73} (ExpS 2.1–2.8; Fig. 4A,B, and Table 1) variants that can interact productively with the TBS in the RPR S-domain (see above). These results are discussed below in "Substrates that can interact productively with the TBS-region—influence of changes of the nucleobase at −1 in substrates and residue 248 in the RPR". Following this we analyzed the impact of N_{-1}/N_{+73} variants in substrates that cannot form a productive interaction with the TBS, $pATSer_{GAAA}$ (ExpS 3.1–3.6; Fig. 4C and Table 1) and pMini3bp (ExpS 4.1–4.12; Fig. 4D and Table 2) variants. These data are discussed in "Substrates that cannot interact productively with the TBS-region—influence of changes of the nucleobase at −1 in substrates and residue 248 in the RPR". In "Altering the WC-surface of a U at position −1 and influence of the N248 identity", we discuss substrates carrying CH_3 at position 3 on the nucleobase that alter the WC-surface of U_{-1} in model substrates

	ExpS	CL site	A_{248} (wt)	RPR variant		
				C_{248}	G_{248}	U_{248}
pMini3bpAG	4.1	+1	0.08 ± 0.001	$0.001 \pm 1 \times 10^{-4}$	5.8 ± 0.6	0.044 ± 0.004
pMini3bpCG	4.2	+1	0.2 ± 0.007	$0.002 \pm 1 \times 10^{-4}$	4 ± 0.3	$0.02 \pm 6 \times 10^{-4}$
		−1	0.03 ± 0.002	$0.0001 \pm 1 \times 10^{-5}$	0.3 ± 0.002	$0.005 \pm 1 \times 10^{-4}$
pMini3bpGG	4.3	+1	$0.001 \pm 7 \times 10^{-5}$	$0.0023 \pm 2 \times 10^{-6}$	$0.003 \pm 4.4 \times 10^{-4}$	$0.001 \pm 3 \times 10^{-5}$
		−1	$0.0006 \pm 2 \times 10^{-5}$	ND	$0.007 \pm 3 \times 10^{-4}$	$0.0008 \pm 1 \times 10^{-5}$
pMini3bpUG	4.4	+1	**16 ± 1**	$0.02 \pm 4.4 \times 10^{-4}$	$0.8 \pm 6.4 \times 10^{-4}$	$0.02 \pm 3.3 \times 10^{-5}$
pMini3bpCA	4.5	+1	0.27 ± 0.07	$0.012 \pm 3.4 \times 10^{-4}$	10 ± 1	0.22 ± 0.014
pMini3bpUA	4.6	+1	3.5 ± 1.2	$0.028 \pm 4.4 \times 10^{-4}$	0.38 ± 0.044	$0.003 \pm 2.2 \times 10^{-4}$
pMini3bpCIno	4.7	+1	1.1 ± 0.057	0.012 ± 0.0055	3.5 ± 0.099	0.12 ± 0.0075
pMini3bpDAPG	4.8	+1	0.026 ± 0.0031	$0.00047 \pm 1 \times 10^{-6}$	1.5 ± 0.43	$0.0052 \pm 4.7 \times 10^{-4}$
pMini3bpInoG	4.9	+1	0.027 ± 0.0023	0.035 ± 0.0033	0.017 ± 0.0033	$0.0033 \pm 6 \times 10^{-4}$
pMini3bpPuG	4.10	+1	$0.0075 \pm 2.5 \times 10^{-4}$	$0.0012 \pm 1.7 \times 10^{-5}$	0.095 ± 0.0014	0.0093 ± 0.0014
pMini3bpUDAP	4.11	+1	0.52 ± 0.064	0.0077 ± 0.0019	0.42 ± 0.0016	0.0079 ± 0.0019
pMini3bp2APG	4.12	+1	$0.0088 \pm 5.5 \times 10^{-4}$	$0.00076 \pm 3 \times 10^{-5}$	0.036 ± 0.0014	$0.0046 \pm 7.7 \times 10^{-4}$

Table 2. Rate of cleavage (k_{app}) of pMini3bp for RPR variants without the C5 protein. The data represent mean ± experimental errors calculated from at least three independent experiments and are expressed as cleavage per min per pmol of RPR. Dependent on RPR substrate combination, between 0.4 and 0.8 μM RPR was used, and 2 nM of substrate in all cases. The reactions were performed at 37 °C in buffer C at 800 mM Mg^{2+} (see "Materials and methods") and the "pMini3bp-N_{248}" combination showing the highest rate is highlighted in bold.

	ExpS	CL site	A_{248} (wt)	RPR variant		
				C_{248}	G_{248}	U_{248}
pATSerUG	2.4	+1	73 ± 2	32 ± 4	61 ± 0.4	11 ± 0.2
pATSer**3m**UG	**5.1**	+1	18 ± 2	8 ± 1	15 ± 0.2	4 ± 0.6
$pATSerUG_{GAAA}$	3.4	+1	22 ± 2	0.6 ± 0.05	13 ± 1	0.04 ± 0.006
		−1	0.4 ± 0.005	0.03 ± 0.002	0.4 ± 0.01	0.01 ± 0.002
pATSer**3m**UG_{GAAA}	**5.2**	+1	6 ± 0.3	0.4 ± 0.05	2 ± 0.1	0.05 ± 0.002
		−1	0.2 ± 0.02	0.04 ± 0.005	0.1 ± 0.01	ND
pMini3bpUG	4.4	+1	16 ± 1	$0.02 \pm 4.4 \times 10^{-4}$	$0.8 \pm 6 \times 10^{-4}$	$0.02 \pm 3.3 \times 10^{-5}$
pMini3bp**3m**UG	**5.3**	+1	1 ± 0.001	0.05 ± 0.001	0.3 ± 0.01	0.02 ± 0.001

Table 3. Rate of cleavage (k_{app}) of as a function of having 3-methyl U at −1. The data represent mean ± experimental errors calculated from at least three independent experiments and are expressed as cleavage per min per pmol of RPR. Dependent on RPR substrate combination, between 0.4 and 0.8 μM RPR was used, and 2 nM of substrate in all cases. The reactions were performed at 37 °C in buffer C at 800 mM Mg^{2+} (see "Materials and methods"). The bold ExpS numbers highlight the substrates with **3mU**.

(ExpS 5.1–5.3; Fig. 6 and Table 3). In each sections (A-C), we summarize the data with respect to the possible interaction between residues A_{248} and −1.

Following this, in "Kinetic constants k_{obs} and k_{obs}/K^{sto} and activation energy as a function of N_{248} identity" we present single turnover kinetic data for cleavage of the model substrate pATSerUG with the different 248 variants. These experiments were performed at different temperatures with the objective to determine the activation energy as a function of the N_{248} identity. In the final "Differential effects due to replacement of the 2′OH at −1 with 2′H or 2′NH_2 in pATSerUG and influence of the N_{248} identity on the charge distribution at the cleavage site", we probe the influence of the N_{248} identity on the charge distribution at the cleavage site.

Substrates that can interact productively with the TBS-region—influence of changes of the nucleobase at −1 in substrates and residue 248 in the RPR. *pSu1 variants* (Fig. 4A and Table 1; ExpS 1.1–1.4): All the −1 variants were cleaved mainly at the +1 site and at the alternative position −1 (Fig. 4A), irrespective of the identity of residue 248. Except for U_{248}, the U_{-1} variant (ExpS 1.4) was cleaved with the highest rate at +1 where $k_{app(+1)}$ was highest for $A_{248(wt)}$. With respect to the wild-type substrate, $pSu1C_{-1}$ (ExpS 1.2), $A_{248(wt)}$ was the most efficient catalyst; the k_{app} values for the other three variants were lower.

For $pSu1A_{-1}$ (ExpS 1.1), changing *Eco* $RPR_{A248(wt)}$ to any of the other nucleobases resulted in decreased cleavage frequency at +1 relative to −1, while comparing k_{app} values for cleavage at +1 and −1 with the different RPRs differed ≤ two-fold. Cleavage of $pSu1C_{-1}$ (ExpS 1.2) at +1 was reduced and increased at −1 using G_{248}, but there

was no apparent difference for the other 248 variants. The increased cleavage at −1 for G_{248} is also noticeable by comparing $k_{app(+1)}$ and $k_{app(-1)}$ values (Table 1). The wild-type A_{248} and G_{248} variant cleaved pSu1G_{-1} at +1 with slightly lower frequencies than C_{248} and U_{248} (ExpS 1.3). Moreover, $k_{app(+1)}$ values for all 248 variants were similar (ExpS 1.3) while k_{app} for cleavage at −1 were higher for $A_{248(wt)}$ and G_{248} compared to C_{248} and U_{248}. Finally, with pSu1U_{-1} (ExpS 1.4) we detected modest differences in cleavage frequency at +1 and $k_{app(+1)}$ (at most 2.6-fold change comparing $A_{248(wt)}$ and U_{248}) while no apparent change in $k_{app(-1)}$ was detected irrespective of RPR. We also noted that the 248 variants cleaved the different pSu1 N_{-1} substrates with low frequencies at other positions in the 5′ leader upstream of site −1 (not shown). Noteworthy, in *E. coli* the wild-type pSu1 has a C at position −1, which pairs with the discriminator base G_{+73} (Fig. 3A) and the C_{-1}/G_{+73} pairing influences cleavage efficiency and site selection, see e.g.[27].

pATSer variants (Fig. 4B and Table 1; ExpS 2.1–2.8): Cleavage of the N_{-1} variants carrying A, C, G and U more or less mirrored the results with pSu1 (cf. ExpS 1.1–1.4 vs. 2.1–2.4). Overall G_{248} cleaved with the highest rates both at +1 (pATSerAG; ExpS 2.1) and at −1 (pATSerGG; ExpS 2.3). Moreover, having a purine at 248 gives a more efficient catalyst compared to when a pyrimidine is present at this position with the exception of the "pATSerCG/G_{248}" combination (ExpS 2.2).

Specifically, first pATSerAG (ExpS 2.1) was cleaved with roughly the same frequencies at +1 by all 248 variants with the possible exception for C_{248}, which cleaved this substrate both at +1 and −1 with a lower rate compared to the other RPR variants. Second, compared to the other RPRs G_{248} cleaved pATSerCG more frequently at −1. This is also reflected in the k_{app} values for cleavage at +1 and −1, while the G_{248} and C_{248} RPRs cleaved pATSerCG at +1 with the same rates (ExpS 2.2). These results are contradictory to the formation of *cis* WC/WC pairing between C_{-1} and G_{248} in the RPR-substrate complex. Third, in contrast there appeared to be suppression/rescue of cleavage of pATSerGG at −1 using C_{248} (comparing frequencies of cleavage at −1 and $k_{app(-1)}$; Fig. 4B and Table 1; cf. ExpS 2.3 C_{248} vs. G_{248}). Fourth, pATSerUG (cf. ExpS 2.4) was almost exclusively cleaved at +1 by all 248 variants (see also Fig. 3F). However, U_{248} cleaved pATSerUG with a significantly lower rate at +1 than the other RPR variants (Table 1).

For the pATSer variants with "unnatural" nucleobases at −1 and +73, reducing the number of potential hydrogen bonds between −1 and +73 from three to two restored cleavage at +1 for G_{248} to the level observed for the other 248 variants (Fig. 4B; cf. ExpS 2.2 and 2.5, i.e. pATSerCG vs. pATSerCIno). This appeared to be the result of an increase in the rate of cleavage at +1 while hardly any effect on the rate was detected for cleavage at −1 (Table 1; cf. ExpS 2.2 and 2.5). By contrast, the potential formation of three hydrogen bonds between U_{-1} and DAP_{+73} resulted in increased miscleavage for all four 248 variants (Fig. 4B; cf. ExpS 2.4 and 2.8, i.e. pATSerUG vs. pATSerUDAP). This was accompanied with noticeable rates of cleavage at −1 (Table 1; cf. ExpS 2.4 and 2.8). In keeping with this, the k_{app} values for cleavage at +1 were lower for pATSerUDAP relative to pATSerUG for all RPR variants.

In summary (see Fig. 5A), (i) when the T-loop can form a productive interaction with TBS in the S-domain we did not detect any conclusive evidence for *cis* WC/WC pairing between N_{-1} and N_{248}. However, for some of the combinations, *cis* WC/WC pairing cannot be excluded (see also the "Discussion"). (ii) The potential to form three H-bonds between N_{-1} and N_{+73} affected both cleavage site selection and dependent on substrate-RPR combination the rate of cleavage. (iii) For *Eco* $RPR_{A248(wt)}$, cleavage of substrates with natural nucleobases at N_{-1}, the U_{-1} substrates are preferred.

Substrates that cannot interact productively with the TBS-region—influence of changes of the nucleobase at −1 in substrates and residue 248 in the RPR. *pATSer GAAA-tetra loop variants* (Fig. 4C and Table 1; ExpS 3.1–3.6): Replacement of the T-loop with a GAAA-tetra loop in the pATSer variants resulted in reduced frequency of cleavage at +1 for several combinations and lower $k_{app(+1)}$ (cf. ExpS 2.1–2.4 vs. 3.1–3.4). However, dependent on substrate-RPR combination the decrease in rate at +1 varied between ≈ two- to 1000-fold; for example the $k_{app(+1)}$ ratio for pATSerCG/pATSerCG$_{GAAA}$ and C_{248} showed a 1000-fold difference, but only ≈two-fold for pATSerCG/pATSerCG$_{GAAA}$ and G_{248} (Table 1; ExpS 2.2 vs. 3.2, cf. k_{app} 10 vs. 0.01 and 11 vs. 5, respectively). For cleavage at −1, the decrease in $k_{app(-1)}$ was lower (≤ 20-fold) in response to substituting the T-loop with GAAA for all four 248 variants except for cleavage of pATSerGG vs. pATSerGG$_{GAAA}$ with C_{248}. Here the decrease in ($k_{app(-1)}$) was > 100-fold (Table 1; ExpS 2.3 vs. 3.3). Moreover, for the "pATSerAG$_{GAAA}$/C_{248}", "pATSerCG$_{GAAA}$/G_{248}" and "pATSerGG$_{GAAA}$/C_{248}" combinations, we did observe significant cleavage at +1 with frequencies (relative to −1) comparable to those with an intact T-loop (e.g. cf. C_{248} cleavage of pATSerAG and pATSerAG$_{GAAA}$; Fig. 4B,C; ExpS 2.1 vs. 4.1). Substitution of the T-loop with the GAAA-tetra loop in pATSerUG increased cleavage at −1 for U_{248}, while we detected only small changes for the other 248 variants including the wild type (cf. Fig. 4B,C; ExpS 2.4 vs. 3.4). However, all RPR variants cleaved pATSerUG$_{GAAA}$ with measurable $k_{app(-1)}$ values in contrast to pATSerUG (Table 1; ExpS 2.4 vs. 3.4). In keeping with the importance of pairing between N_{-1} and N_{+73} (see above) changing G to A at +73 in pATSerCG$_{GAAA}$ restored cleavage at +1 with increased rates irrespective of N_{248} variants (Fig. 4C and Table 1; cf. pATSerCG$_{GAAA}$ vs. pATSerCA$_{GAAA}$, ExpS 3.2 and 3.5). By contrast, comparing $k_{app(+1)}$ values for cleavage of pATSerUG$_{GAAA}$ and pATSerUA$_{GAAA}$ showed the opposite, i.e., lower $k_{app(+1)}$ irrespective of 248 variant (Table 1; ExpS 3.4 vs. 3.6). For pATSerUA$_{GAAA}$, increased frequency of cleavage at −1 was detected with U_{248} and it also cleaved pATSerUA$_{GAAA}$ at position −2 (≈20%) in the 5′ leader. Finally, a comparison of $k_{app(+1)}$ values (and to some extent also $k_{app(-1)}$) suggested that $A_{248(wt)}$ and G_{248} were more efficient catalysts than C_{248} and U_{248} when pATSerNN$_{GAAA}$ variants were used.

pMini3bp variants (Fig. 4D and Table 2; ExpS 4.1–4.12): For the variants with natural nucleobases at −1 we did observe significant reduction in cleavage of the G_{-1} variant at +1 using $A_{248(wt)}$, G_{248} and U_{248} while C_{248} cleaved the G_{-1} substrate preferentially at +1 (Fig. 4D; ExpS 4.3). Moreover, irrespective of 248 variants pMini3bpCG and pMini3bpCA were cleaved mainly at +1 with some cleavage at −1 and cleavage of pMini3bpUA was detected only

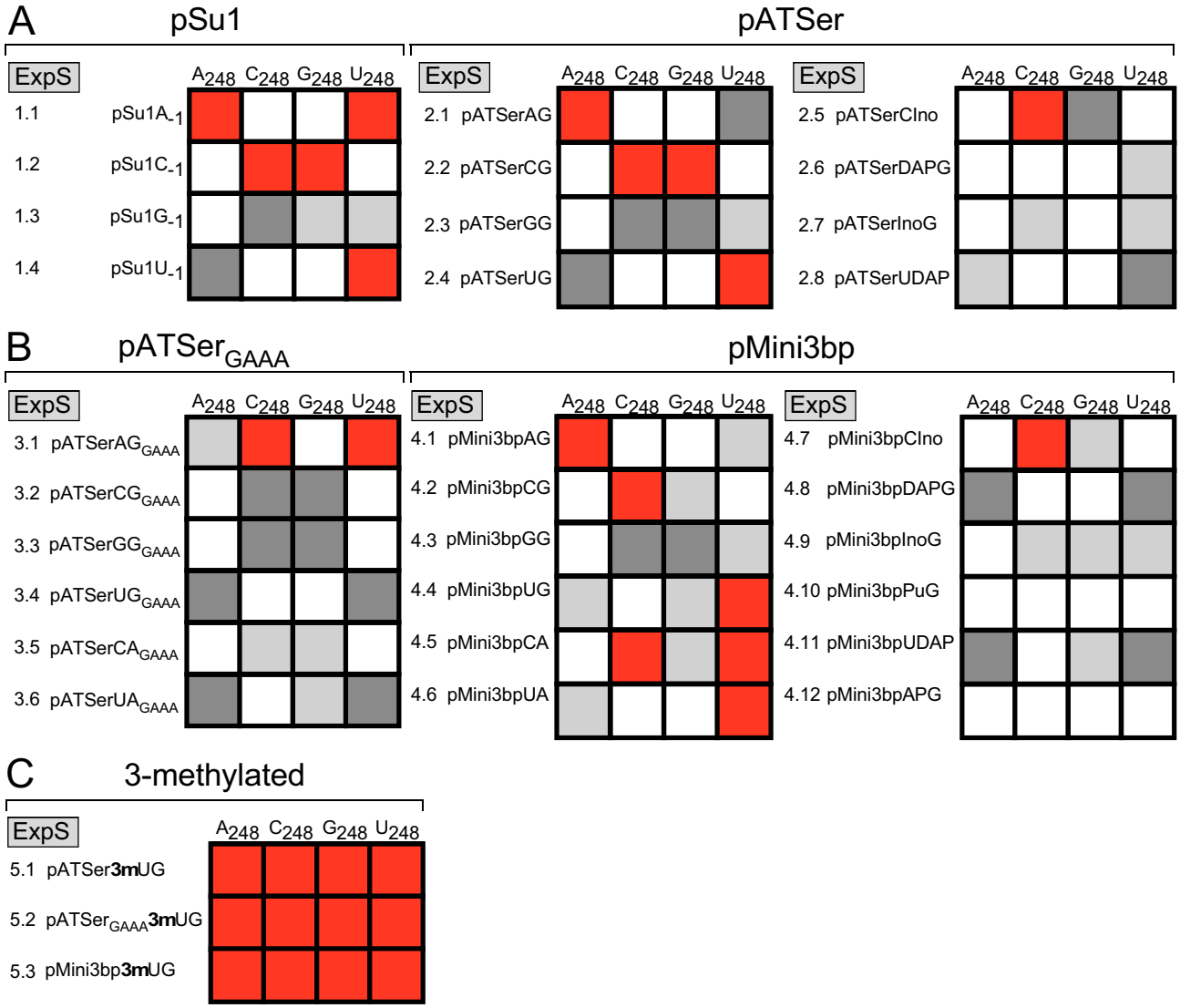

Figure 5. Summary of data for N_{-1}/N_{248} *cis* WC/WC base paring. Boxes marked in gray are consistent with *cis* WC/WC base-pairing; light gray marks those combinations where one combination (or weak agreement/non-WC/WC pairing e.g. GU-pairing) are consistent with *cis* WC/WC base-pairing, e.g. cf. $pSu1U_{-1}/A_{248}$- vs $pSu1A_{-1}/U_{248}$-combinations. Boxes marked in red highlight the combinations that are not in agreement with *cis* WC/WC base pairing, while no color indicates other combinations. The grey ExpS boxes refer to the Experimental Series, e.g. 1.1–1.4 and 2.1–2.8 etc., as shown in Figs. 4 and 6, and Tables 1, 2 and 3. (**A**) Experiment series using pSu1 (ExpS 1.1–1.4) and pATSer (ExpS 2.1–2.8) variants, which can establish a productive interaction with the TBS region in the S-domain (see main text for details). (**B**) Experiment series using pATSerGAAA (ExpS 3.1–3.6) and pMini3bp (ExpS 4.1–4.12) variants, which cannot form a productive interaction with the TBS region in the S-domain (see main text for details). (**C**) Experiment series for model substrates with a 3-methyl group at U_{-1} (ExpS 5.1–5.3).

at +1 (Fig. 4D; ExpS 4.2, 4.3 and 4.5). The other three variants, pMini3bpAG, pMini3bpUG and pMini3bpUA (ExpS 4.1, 4.4 and 4.6), were cleaved almost exclusively at +1 by all four 248 variants.

With respect to the rate of cleavage we compared $k_{app(+1)}$ (except for two substrates, see below) because the rates were significantly lower than for the other substrates, in particular at −1 (Table 2). Overall, $k_{app(+1)}$ for $A_{248(wt)}$ and G_{248} were higher compared to C_{248} and U_{248}; the highest $k_{app(+1)}$ was for pMini3bpUG (ExpS 4.4) with $A_{248(wt)}$. This is in keeping with the trend seen with the other substrate variants, i.e. U_{-1} variants were in general cleaved with the highest rates at +1 (but cf. e.g., the "pATSerAG/G_{248}" combination above). For the "pMini3bpCG/G_{248}" combination (ExpS 4.2), $k_{app(+1)}$ and $k_{app(-1)}$ were both higher than when the other 248 variants, including $A_{248(wt)}$, were used. Comparing cleavage of pMini3bpCG vs. pMini3bpGG (ExpS 4.2 and 4.3) with G_{248}, $k_{app(+1)}$ was ≈1300-fold higher for pMini3bpCG, while $k_{app(-1)}$ was ≈40-fold higher. No difference in $k_{app(+1)}$ was detected for C_{248} cleaving these two substrates, while $k_{app(-1)}$ was 3000-fold lower in cleaving pMini3bpCG than when G_{248} was used (Table 2; ExpS 4.2 and 4.3, cf. 0.0001 vs. 0.3). In fact, C_{248} was found to be a very poor catalyst with all pMini3bp substrates. Analyzing the (pMini3bpUG and pMini3bpAG)/$A_{248(wt)}$ and (pMini3bpUG and pMini3bpAG)/U_{248} combinations (ExpS 4.1 and 4.4) revealed a significant drop in $k_{app(+1)}$ for $A_{248(wt)}$ by replacing U_{-1} with A_{-1}, but

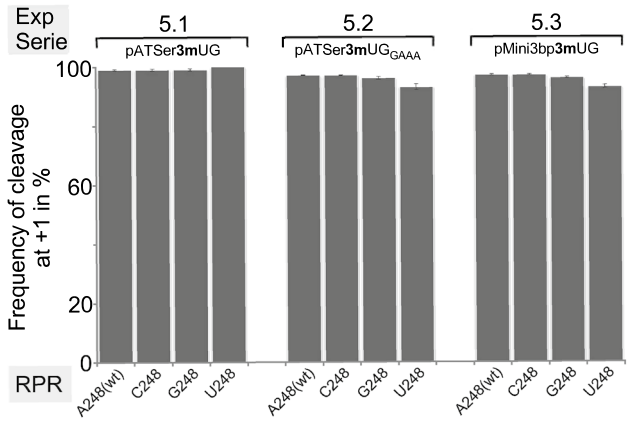

Figure 6. Frequencies of cleavage-site selection for 3-methylated substrates by *Eco* RPR 248 variants. Histograms summarizing frequencies of cleavage at +1 in % during *Eco* RPR-mediated cleavage of pATSer**3m**UG (ExpS 5.1), pATSer**3m**UG_{GAAA} (ExpS 5.2) and pMini3bp**3m**UG (ExpS 5.3) as indicated. We used the 5′ cleavage fragments to calculate the frequencies of cleavage at +1; mean and experimental errors were calculated from at least three independent experiments.

only a two-fold rescue (cf. pMini3bpUG vs. pMini3bpAG) using U_{248}. Interestingly, G_{248} cleaved the pMini3bpAG substrate at +1 with a markedly higher rate ($k_{app(+1)}$) compared to using the other 248 variants (Table 2; ExpS 4.1).

For the variants carrying "unnatural" nucleobases at −1 and/or at +73, most combinations resulted in cleavage mainly at +1 (Fig. 4D). The most apparent exceptions were for the combinations "pMini3bpDAPG/$A_{248(wt)}$", "pMini3bp2APG/$A_{248(wt)}$", and "pMini3bpUDAP/U_{248}".

The pMini3bp variants cannot interact with the TBS-region (see above) and comparison of the pATSer (with T-loop) and the pMini3bp data sets (cf. Fig. 4B,D) revealed that some pATSer variants such as pATSerAG (ExpS 2.1), pATSerInoG (ExpS 2.7) and pATSerUDAP (ExpS 2.8; except U_{248}) were cleaved at −1 with higher frequencies by all four 248 variants. Relative to cleavage of the pATSer derivatives with GAAA-tetra loops, the frequencies of cleavage at +1 were, in general, higher with the pMini3bp variants.

Considering rates of cleavage, introduction of $2NH_2$ [Table 2; cf. pMini3bpAG (ExpS 4.1) vs. pMini3bpDAPG (ExpS 4.8)] and removal of the $6NH_2$ [Table 2; cf. pMini3bpAG (ExpS 4.1) vs. pMini3bp2APG (ExpS 4.12)] on the −1 nucleobase resulted in a ≈four- and ≈ 160-fold decrease in $k_{app(+1)}$ for G_{248}, while for $A_{248(wt)}$ the corresponding values were ≈ three- and ≈ ten-fold lower. These data suggested that in particular the exocyclic amine at position 6 on A_{-1} plays a more important role for cleavage with G_{248} than for $A_{248(wt)}$. Cleavage of pMini3bpUG and pMini3bpUA with G_{248} resulted in a 20- and ten-fold lower $k_{app(+1)}$, respectively, compared to $A_{248(wt)}$ (Table 2; ExpS 4.4 and 4.6) while only a small difference in $k_{app(+1)}$ was detected for cleavage of pMini3bpUDAP using these two RPRs (Table 2; ExpS 4.11). Moreover, the $k_{app(+1)}$ values for these three pMini3bp U_{-1} substrates using G_{248} were similar, within a factor of two. This might indicate that the catalytic performance of $A_{248(wt)}$ is influenced by pairing between N_{-1} and N_{+73} and/or the pairing between N_{+73} and U_{294} in the RPR-substrate complex.

In summary (see Fig. 5B), (i) the cleavage site distribution data did not provide any conclusive evidence for *cis* WC/WC pairing between residues N_{-1} and 248 in the *Eco* RPR substrate complex when we interfered with/or removed the interaction between the T-loop and TBS. However, there were a few possible exceptions, e.g., the combinations "pATSerCG_{GAAA}/G_{248}", "pATSerGG_{GAAA}/C_{248}", and "pMini3bpGG/C_{248}". (ii) As in cleavage of pSu1 and pATSer variants, the potential pairing between N_{-1} and N_{+73} influence the efficiency of cleavage and site selection also in the absence of a productive interaction between the T-loop and TBS in the RPR. (iii) Interfering with the interaction between TSL and TBS affect choice of cleavage site and rate of cleavage, see also[15,37].

Together the combined data with the four different substrate series suggested that the influence of N_{-1} and N_{+73} on cleavage site recognition and rate of cleavage at +1 and −1 depend on substrate and/or "N_{-1}/N_{+73}-N_{248}" combination. Moreover, in general we do detect larger variations in k_{app} for cleavage at +1 than at −1. It therefore appears that the impact of the various changes either in the substrate or in the RPR is larger for cleavage at the correct position +1 than at −1. We also emphasize that the choice of cleavage site did not change during the course of the reactions as revealed from the time course experiments used to determine k_{app} values.

Altering the WC-surface of a U at position −1 and influence of the N_{248} identity. To further understand the importance of the Watson–Crick surface of the N_{-1} residue in the substrate we used substrates carrying substitutions of U with 3-methyl U (**3mU**) at −1. This modification would be expected to disturb the interaction with the Watson–Crick surface of U_{-1} (Fig. 3B–E). The data are shown in Fig. 6 and Table 3 (ExpS 5.1–5.3 vs. 2.4, 3.4 and 4.4).

A comparison of cleavage of pATSerUG vs. pATSer**3m**UG revealed no (or very minor) change in choice of cleavage site (Figs. 4B and 6; cf. ExpS 2.4 vs. ExpS 5.1) for any of the four 248 variants. However, $k_{app(+1)}$ dropped three- to four-fold for all four RPRs, with U_{248} being the least efficient catalyst (Table 3).

With pATSerUG$_{GAAA}$, introduction of **3mU** at −1 did not result in any apparent change in cleavage site preference with the notable exception for U_{248}. Here we did detect an increase of cleavage at +1 compared to cleavage of pATSerUG$_{GAAA}$ (Figs. 4C and 6; cf. ExpS 3.6 vs. ExpS 5.2). The other three 248 variants cleaved both pATSerUG$_{GAAA}$ and pATSer**3m**UG$_{GAAA}$ at +1. As for pATSerUG, the presence of **3mU**$_{-1}$ influenced cleavage rates; $k_{app(+1)}$ values were down four- to six-fold using $A_{248(wt)}$ and G_{248}, respectively, while for C_{248} the decrease was very modest, ≈1.5-fold. No apparent change was detected for U_{248}. Interestingly, **3mU**$_{-1}$ influenced the rate of cleavage at +1 for $A_{248(wt)}$ and C_{248} while cleavage by G_{248} resulted in a four-fold decrease (Table 3; cf. ExpS 3.4 vs. ExpS 5.2).

Comparing cleavage of pMini3bpUG vs. pMini3bp**3m**UG, we detected just a small increase in cleavage at −1 for all 248 variants (Figs. 4D and 6; cf. ExpS 4.4 vs. ExpS 5.3). Moreover, $k_{app(+1)}$ for $A_{248(wt)}$ was down 16-fold in response to the introduction of **3mU**$_{-1}$. For G_{248} and C_{248}, the change was more modest, 2.7-fold lower for G_{248} while C_{248} cleaved **3mU**$_{-1}$ with a 2.5-fold higher rate than it cleaved the corresponding substrate lacking the methyl modification. No change was detected for U_{248}.

In summary (see Fig. 5C), the presence of **3mU**$_{-1}$ that blocks the Watson–Crick surface has an impact on the rate of cleavage. The impact on the rate at +1 ($k_{app(+1)}$) appears to be dependent on RPR-substrate combination, as exemplified by cleavage of pMini3bpUG and pMini3bp**3m**UG with $A_{248(wt)}$ vs. C_{248}. Remarkably, introduction of **3mU**$_{-1}$ in the "pATSer-GAAA-tetra-loop" substrate rescued cleavage at +1 using the U_{248} RPR variant. Hence, these findings do not support *cis* WC/WC pairing between N_{-1} and 248 for these substrates, see also[29].

Kinetic constants k_{obs} and k_{obs}/K^{sto} and activation energy as a function of N_{248} identity. The data presented above clearly suggested that the identity of residue 248 affect both cleavage site recognition and rate of cleavage. We therefore decided to determine the kinetic constants, k_{obs} and k_{obs}/K^{sto} (for cleavage at +1), for the different 248 variants using pATSerUG. To gain insight into why a purine at 248 (in particular A at 248) is preferable over a pyrimidine, we also determined k_{obs} and k_{obs}/K^{sto} at different temperatures. This would allow us to estimate the activation energy for the reaction catalyzed by the various 248 RPRs. These series of experiments were done under single turnover conditions at 800 mM Mg^{2+} (see above) and the results are shown in Fig. 7 and Table 4.

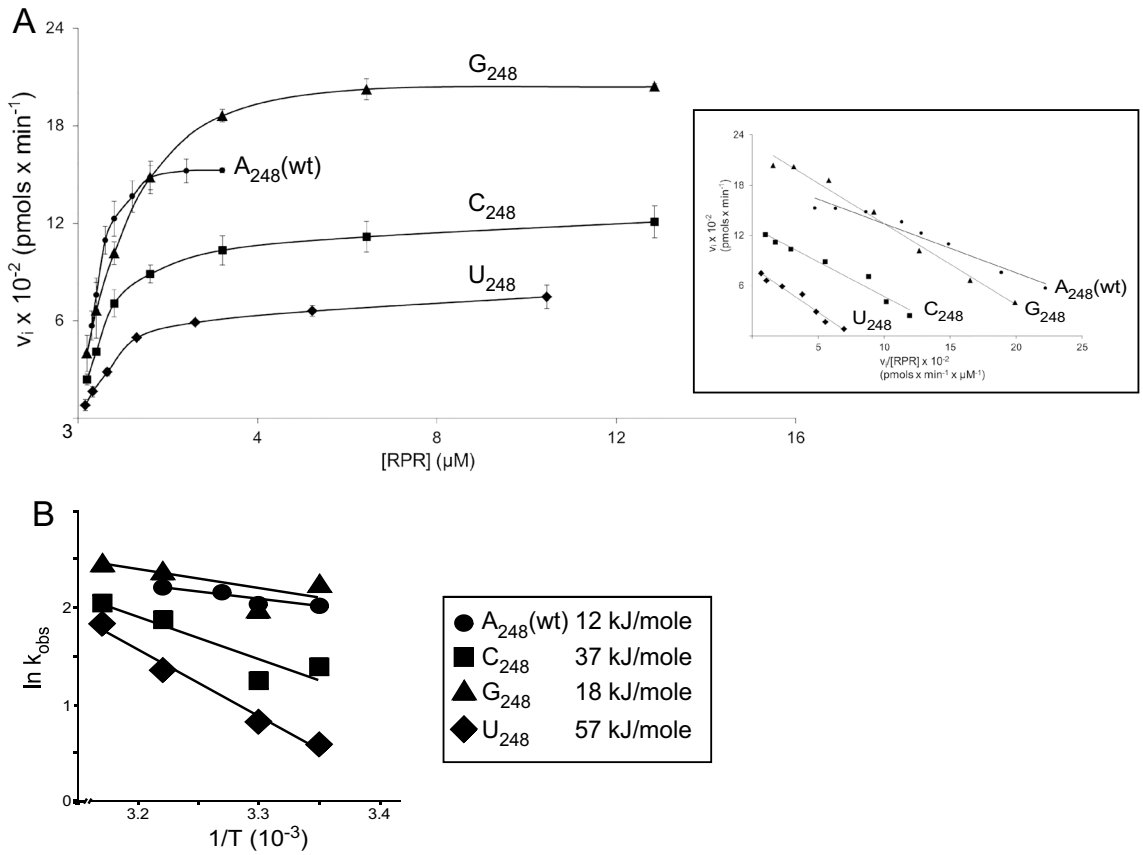

Figure 7. Kinetics of cleavage of pATSer with the *Eco* RPR 248 variants and Arrhenius plots. (**A**) Rate of cleavage of pATSerUG as a function of increasing concentration of the *Eco* RPR 248 variants. The experiments were performed at 37 °C in buffer C containing 800 mM Mg^{2+} as described in "Materials and methods". The data represent mean and experimental errors from at least three independent experiments. Insets correspond to Eadie–Hofstee plots using the primary data and the k_{obs} and k_{obs}/K^{sto} values presented in Table 4. (**B**) Arrhenius plots of temperature dependence of k_{obs} for the *Eco* RPR_{248} variants as indicated. The data are summarized in Table 4 and the temperatures are in Kelvin. The values given in the inset correspond to the calculated E_a (activation energy) values.

248 variant	Temp (°C)	k_{obs} (min^{-1})	k_{obs}/K^{sto} (min^{-1} μM^{-1})	$K^{sto} \approx K_d$ (μM)	E_a (kJ mol^{-1})
A_{248}	25	7.6 ± 0.32	9.3 ± 2.6	0.9 ± 0.29	12
	30	7.7 ± 0.5	11 ± 1	0.7 ± 0.024	
	33	8.6 ± 0.27	7.2 ± 0.44	1.2 ± 0.039	
	37	9.1 ± 0.035	16 ± 3.4	0.6 ± 0.12	
C_{248}	25	4.0 ± 0.37	5.2 ± 1.6	0.92 ± 0.42	37
	30	3.5 ± 0.25	7.4 ± 1.8	0.51 ± 0.14	
	37	6.5 ± 0.10	7.9 ± 0.63	0.84 ± 0.066	
	42	7.8 ± 0.41	14 ± 1.3	0.58 ± 0.069	
G_{248}	25	9.4 ± 0.24	16 ± 2	0.6 ± 0.094	18
	30	7.4 ± 0.49	8.3 ± 3.5	1.3 ± 0.75	
	37	11 ± 0.44	13 ± 3.6	1 ± 0.27	
	42	12 ± 0.18	16 ± 1.5	0.78 ± 0.078	
U_{248}	25	1.8 ± 0.066	3.2 ± 0.4	0.55 ± 0.054	57
	30	2.3 ± 0.21	6.1 ± 0.36	0.37 ± 0.057	
	37	3.9 ± 0.21	3.6 ± 0.42	1.1 ± 0.16	
	42	6.3 ± 0.18	6 ± 0.73	1.1 ± 0.18	

Table 4. The kinetic constants for cleavage of pATSerUG at as a function of temperature and 248 variant. The experiments were performed under single-turnover conditions at 800 mM Mg^{2+} concentrations at pH 6.1 as outlined in "Materials and methods". For details regarding the calculation of K_d, see the main text, Wu et al.[31] and references therein. The activation energies were calculated using the k_{obs} values as described in Tallsjö and Kirsebom[68] (see also Fig. 7). The data represent mean ± experimental errors calculated from at least three independent experiments.

The k_{obs} and k_{obs}/K^{sto} values for $A_{248(wt)}$ at 37 °C agreed with our previous data (Table 4)[37]. A comparison of k_{obs} and k_{obs}/K^{sto} for the four 248 variants revealed that having A or G at 248 resulted in the most efficient catalysts, in agreement with data discussed above. For $A_{248(wt)}$, lower temperature resulted in a modest but reproducible decrease in k_{obs}. This trend was also detected for the other 248 variants. The k_{obs} at different temperatures were highest for $A_{248(wt)}$ and G_{248}, and lowest for C_{248} and U_{248}. Irrespective of 248 variant and temperature, the K^{sto} values were similar within a ≈ two- to three-fold range. We have argued that under these reaction conditions $K^{sto} \approx K_d$ (see "Materials and methods")[31] and references therein. On the basis of this, our data suggested that substituting $A_{248(wt)}$ resulted in a modest change in binding affinity for pATSerUG.

Notwithstanding that the variation in k_{obs} in response to temperature was modest (but reproducible) we plotted k_{obs} as a function of temperature (Arrhenius plot). This would give an indication about the activation energy (E_a) for cleavage of pATSerUG by the different 248 variants. The E_a values varied from 12 to 57 kJ/mole, with $A_{248(wt)}$ having the lowest value followed by $G_{248} < C_{248}$ and $< U_{248}$ (Fig. 7; Table 4).

Taken together, in keeping with the data discussed above, a purine at 248 is preferred over a pyrimidine, with U_{248} being the weakest catalyst. From these data it also appears that this is, at least in part, due to the activation energy barrier being lower with a purine at 248, in particular with an adenosine as in *Eco* $RPR_{A248(wt)}$. This provides one rational why A at position 248 in bacterial RPR (*Eco* numbering) is conserved (see also the "Discussion").

Differential effects due to replacement of the 2′OH at −1 with 2′H or $2'NH_2$ in pATSerUG and influence of the N_{248} identity on the charge distribution at the cleavage site. The 2′OH of residue −1 is important for both cleavage rates and site selection in bacterial RPR-mediated catalysis[43]. Hence, we decided to investigate whether replacement of the U_{-1} 2′OH with 2′H or $2'NH_2$ in pATSerUG (pATSer**d**UG and pATSer**am**UG, respectively; Fig. 3B,E) influenced the choice of cleavage site.

Introduction of a 2′H (pATSer**d**UG) resulted in reduced cleavage at +1 for all 248 variants irrespective of pH (5.2, 6.1 and 7.2) consistent with previous data using pre-tRNA[24,25]. Importantly, cleavage at −1 did not increase with pH (Fig. 8A). Cleavage of the $2'NH_2$ substituted substrate (pATSer**am**UG) on the other hand resulted in increased cleavage at +1 at higher pH. In contrast to cleavage with $A_{248(wt)}$ and G_{248} higher pH was required to reach 50% cleavage at +1 using C_{248} (Fig. 8B). The most dramatic effect however, was observed using the U_{248} variant. Here we did not detect any significant change in the frequency of cleavage at +1 with increasing pH.

The pH dependent cleavage of pATSer**am**UG at +1 by *Eco* $RPR_{A248(wt)}$ is also influenced by the identity of N_{+1}/N_{+72} (cf. Fig. 5 in[40]; see also[44]; Fig. 8B,C; cf. G_{+1}/C_{+72}, A_{+1}/U_{+72}, $2AP_{+1}/U_{+72}$, DAP_{+1}/U_{+72} and Ino_{+1}/C_{+72} substrate variants). This was also the case for the C_{248} and G_{248} variants. Of those substrate variants having an exocyclic amine at position 2 on the nucleobases ($2NH_2$) at +1 (Fig. 3B; cf. substrates with G_{+1}, $2AP_{+1}$ and DAP_{+1}) C_{248} showed a similar response to pH as $A_{248(wt)}$, while higher pH was needed to reach 50% cleavage at +1 for G_{248} except using pATSer**am**UG(G_{+1}/C_{+72}) (cf. Fig. 8A–C). For the substrates lacking a $2NH_2$ on the nucleobase at +1 [pATSer**am**UG(A_{+1}/U_{+72}) and pATSer**am**UG(Ino_{+1}/C_{+72})], we detected only a small increase in cleavage at +1 with increasing pH for $A_{248(wt)}$, C_{248} and G_{248} while for U_{248} no cleavage at +1 was observed. In fact, for U_{248} we observed no or only a small increase in cleavage at +1 using all pATSer**am**UG(N_{+1}/N_{+72}) variants with increasing

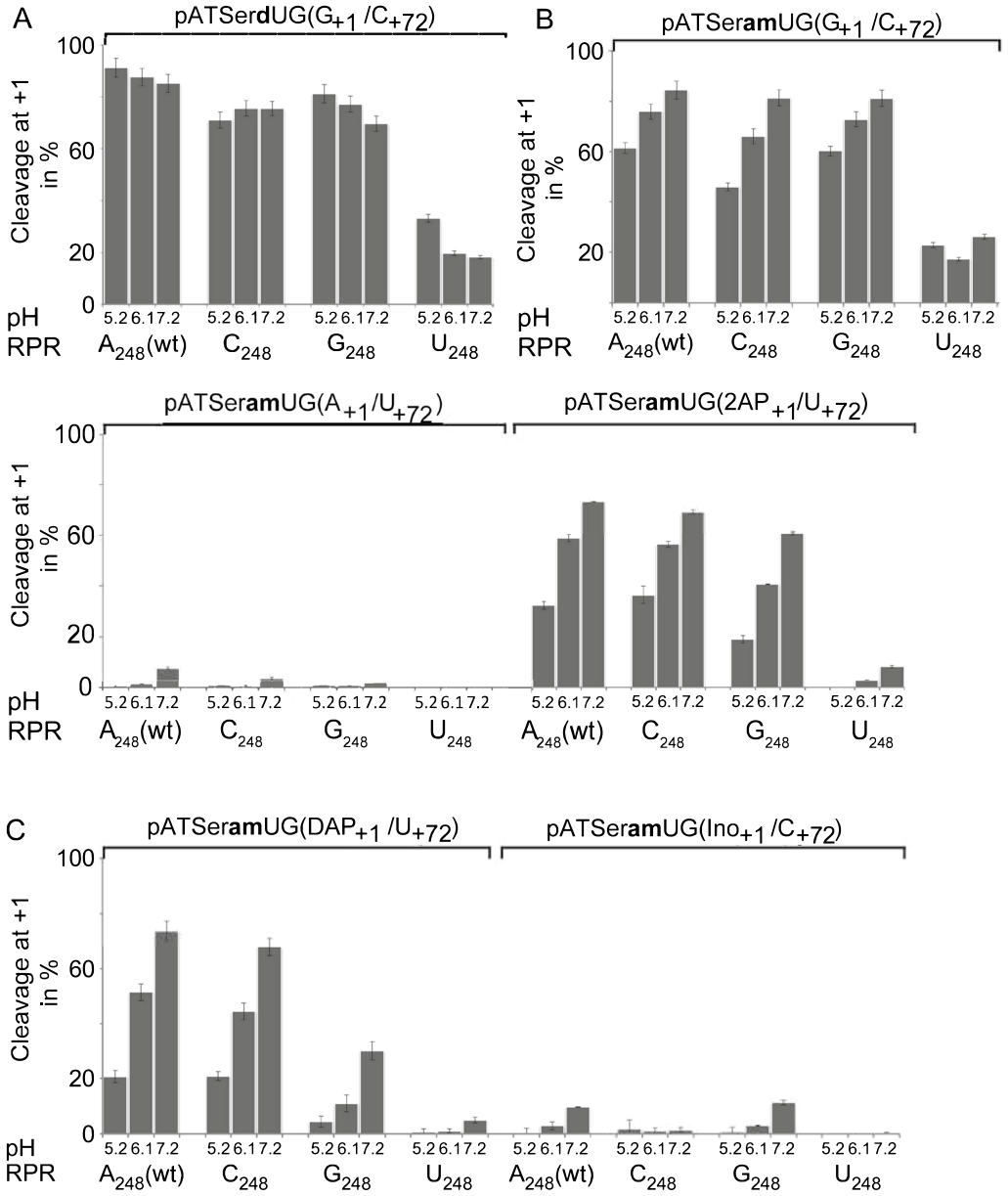

Figure 8. Frequencies of cleavage at +1 of different pATSerUG derivatives with 2′H or 2′NH_2 at the −1 position at different pHs by *Eco* RPR 248 variants. (**A**) Histograms summarizing frequencies of cleavage at +1 in % during *Eco* RPR-mediated cleavage of pATSer**d**UG (2′OH at −1 substituted with 2′H). (**B**) Histograms summarizing frequencies of cleavage at +1 in % during *Eco* RPR-mediated cleavage of pATSer**am**UG (2′OH at −1 substituted with 2′NH_2) and pATSer**am**UG(2AP_{+1}/U_{+73}). (**C**) Histograms summarizing frequencies of cleavage at +1 in % during *Eco* RPR-mediated cleavage of pATSer**am**UG(A_{+1}/U_{+73}) and pATSer**am**UG(2AP_{+1}/U_{+73}). (**D**) Histograms summarizing frequencies of cleavage at +1 in % during *Eco* RPR-mediated cleavage of pATSer**am**UG(DAP_{+1}/U_{+73}) and pATSer**am**UG(Ino_{+1}/C_{+73}). We used the 5′ cleavage fragments to calculate the frequencies of cleavage at +1 at different pH as indicated; mean and experimental errors were calculated from at least three independent experiments. For experimental details see "Materials and methods".

pH. For all the RPR substrate combinations we also detected cleavage at other positions both downstream of the +1 site and in the 5′ leader with increasing pH (not shown). Also, irrespective of residue at 248 no significant change in the frequencies of cleavage at +1 with changing pH using the all ribo substrate variants was detected (not shown).

Taken together, these data suggest that the protonation (the pKa value) of the 2′NH_2 at −1 is affected by the nucleobase identity at position 248 in *Eco* RPR and at +1 (and +72) in pATSerUG (see "Discussion").

Discussion

Residues in the RNase P substrate interact with several regions of the RNA subunit (RPR) of bacterial RNase P (see introduction). Among these the N_{-1} residue in the substrate 5′ leader is close to the active center where cleavage occurs, and it has been proposed that the well conserved $A_{248(wt)}$ forms a *cis* WC/WC base pair when U is present at −1[24,25]. These studies were primarily based on using pre-tRNAs carrying different deoxyribonucleobases at position N_{-1}. In *E. coli* ≈40% of the pre-tRNAs do not carry a U at −1[24,27,28]. Also, cross-linking studies suggest that N_{-1} and N_{+1} in the substrate are positioned close to A_{248}-C_{253} and G_{332}-A_{333} (*E. coli* numbering, see Fig. 1A)[26,45,46]. Hence, we have argued that $A_{248(wt)}$ is a key nucleobase of a N_{-1} binding surface/pocket[16,27,29]. Here we provide data where we analyzed cleavage as a function of $A_{248(wt)}$ substitutions and N_{-1} nucleobase identity using all ribo pre-tRNA and three all ribo model substrates to investigate whether N_{-1} and N_{248} forms a *cis* WC/WC base pair. If *cis* WC/WC base pair forms between N_{-1} and N_{248} this means that the phenotypic change due to disruption of the N_{-1}/N_{248} pairing can be rescued by a compensatory change that restores pairing between N_{-1}/N_{248}. For the pre-tRNA substrate pSu1 and the model substrate pATSer, which both can form a productive TSL/TBS-interaction (see "Introduction", induced fit mechanism)[15,30,37,46], the data supported *cis* WC/WC pairing for substrates carrying G at −1, while we did not find any conclusive evidence for *cis* WC/WC pairing using the other combinations (except the U_{-1}/A_{248} vs. A_{-1}/U_{248} combinations in the pATSer context; see summary, Fig. 5A). When we interfered with the TSL/TBS-interaction by using "pATSer-GAAA-tetra-loop" substrates our findings are consistent with *cis* WC/WC pairing using the C_{-1}, G_{-1} and U_{-1} substrate variants but not for A_{-1} (see summary, Fig. 5B). The impact of the N_{-1}/N_{248} interaction was also detected using pre-tRNA substrates carrying a 2′H at −1 or substrates that could not form the RCCA-RNase P RNA interaction[24,25], i.e. when additional RPR substrate interactions were disrupted. Moreover, our findings with the pMini3bp variants, which cannot interact with TBS in the S domain, lend less support for *cis* WC/WC pairing than when the "pATSer-GAAA-tetra-loop" series was used. But, support comes from using pMini3bpGG, pMini3bpDAPG and pMini3bpUDAP, where the latter can form three hydrogen bonds between N_{-1} and N_{+73} in the substrate (see summary, Fig. 5B). In summary, detection of possible *cis* WC/WC pairing between N_{-1} and N_{248} depends on substrate and disruption of more than one RPR-substrate contact such as the TSL/TBS-interaction.

Residue A_{248} is well conserved among bacterial RPRs and if the U_{-1} WC surface are involved in pairing with residue $A_{248(wt)}$ blocking the N3 position on the nucleobase—by adding a methyl group (**3mU**)—would interfere with choice of cleavage site and rate of cleavage. As in pSu1, the model substrates carry an A at −2. Hence, following Zahler et al.[24,25], who used pre-tRNA^{Asp} that also carries A_{-2}, we argued that interfering with the formation of the "$U_{-1}/A_{248(wt)}$" potential pairing would result in a shift of cleavage from the correct site to the alternative site −1 due to the presence of the 3-methyl group at the N3 position of U_{-1} in the substrate. All three **3mU**$_{-1}$ model substrate variants were, however, preferentially cleaved at +1 irrespective of 248-variant. This is inconsistent with *cis* WC/WC pairing (see summary, Fig. 5C). Importantly, the introduction of **3mU**$_{-1}$ in the three all ribo model hairpin loop substrates did not shift choice of cleavage site for wild type *Eco* $RPR_{A248(wt)}$, which would be expected if there was *cis* WC/WC pairing between U_{-1} and $A_{248(wt)}$, see also[29]. It is also noteworthy that the presence of **3mU**$_{-1}$ in the "pATSer-GAAA-tetra-loop" substrate rescued cleavage at +1 using the U_{248} RPR variant. Together these data do not support *cis* WC/WC pairing between U_{-1} and $A_{248(wt)}$ in wild type *Eco* RPR. In this context we emphasize that substituting $A_{248(wt)}$ with U influenced the structure of the RPR, in particular in the P18 region, which has a role in connecting the S- and the C-domains. The P18 loop interacts with P8 and disruption of this interaction affects cleavage efficiency of both pre-tRNAs and model hairpin loop substrates[47–51]. Hence, this structural change in the RPR might therefore have an impact on the catalytic performance of the U_{248} variant, both with respect to site selection and rate of cleavage; however, again this would be substrate dependent. This would be in keeping with a perturbed coupling (i.e. induced fit, see e.g. Ref.[15]) between a productive TSL-TBS interaction and events at the cleavage.

Furthermore, in *E. coli* as well as in other bacteria a U is the most frequently (≈60%) occurring nucleobase at −1 in pre-tRNA 5′ leaders[24,25,27,28]. This also applies to the archaea *Pyrococcus furiosus* (65% U_{-1}), which as *E. coli* possess a type A RPR and an A at the corresponding position to A_{248}[9,12,22] (Fig. 1B). As discussed above, there is limited support for *cis* WC/WC pairing between U_{-1} and $A_{248(wt)}$ in wild type *Eco* RPR. High GC-content bacteria such as *Mycobacterium tuberculosis* (and other mycobacteria; see Fig. 1B) and *Neisseria meningitides* carry type A RPRs with $A_{248(wt)}$ (*E. coli* numbering). In these bacteria, C at −1 is the most frequently occurring nucleobase, while U_{-1} is present in ≈13% and ≈32% of the pre-tRNAs, respectively[27,28]. This argues against formation of *cis* WC/WC pairing between N_{-1} and $A_{248(wt)}$ for the majority of pre-tRNAs in these bacteria.

In conclusion for the majority of pre-tRNAs (and model substrates), A_{248} does not interact with N_{-1} via *cis* WC/WC pairing. However, given that RNase P processes other RNA transcripts, including mRNAs[2], we cannot completely exclude the possibility that $A_{248(wt)}$ is engaged in *cis* WC/WC pairing with these substrates. In this context we also have to consider that our experiments were performed without the C5 protein and hence the presence of C5 might have an impact given that C5 interact with residues upstream of N_{-1} (see above[41,42]). We propose that the structural architecture of the "active site" is flexible and varies dependent on the identity of the nucleobases at and near the cleavage site and their potential to interact with chemical groups in the RPR. This flexibility is also predicted to depend on the interaction between the pre-tRNA TSL-region and its binding site (TBS) in the RPR S-domain (see above) as well as the RCCA-RPR interaction[15,24,25,30,37,44,46].

Structural architecture and Me(II)-binding near the cleavage site. RNase P mediated cleavage depends on Me(II)-ions, which are involved in activating the water molecule that acts as the nucleophile, substrate interaction and folding of the RPR[43,52]. On the basis of correctness and rate of cleavage available data suggest that Mg^{2+} is the preferred ion. Perreault and Altman[53,54] suggested that binding of Mg^{2+} at the junction between the single stranded 5′ leader and the amino acid acceptor stem involves the two 2′ hydroxyls at positions −1

and −2 forming a productive complex that acts as the true RNase P substrate, see also[25,38,39,46,55,56]. In RNA the structural topology of Me(II)-binding sites affects both binding affinity and positioning of the Me(II)-ion. This is evident from lead(II)-induced cleavage studies of yeast $tRNA^{Phe}$ and *Eco* RPR[15,57–59]. For model substrates, introduction of U_{+1} (or C_{+1}) in pATSerUG (or pATSerCG) affects lead(II)-induced cleavage at the cleavage site such that the frequency of cleavage 5′ of N_{+1} increases more than when a purine is present at +1[60]. Similarly, substituting the 2′OH at -2, −1 and "C_{+74}" in a model hairpin loop model substrate influences Mg^{2+}-induced cleavage between −3 and −2[53]. In keeping with this, substituting the N_{-1} 2′OH with 2′NH_2 in pATSerUG prevent Pb^{2+}-induced cleavage between residue −1 and +1 (not shown). Also, the presence of a 2′NH_2 at N_{-1} in pATSerUG (and pATSerCG) result in a shift of cleavage from −1 to +1 with increasing pH[38–40,44]; this report. The pKa for 2′NH_2 is 6.0–6.2 (determined by NMR-spectroscopy using a dinucleotide)[61,62]. Therefore the 2′NH_2 at −1 in pATSer**am**UG is most likely protonated at lower pH. As a consequence, this results in a positive charge at the +1 cleavage site, which interferes with cleavage at +1, causing the cleavage to shift to −1[38,39]. With increasing pH, the 2′NH_3^+ becomes deprotonated, resulting in cleavage at +1. The pH dependent shift of cleavage from −1 to +1 (i.e., de-protonation of the 2′NH_3^+ at −1) is also dependent on the structure of the N_{+1}/N_{+72} base pair[40]; this report. The data presented here using the 2′NH_2 substituted substrates suggest that the identity of residue 248 in the RPR also influences the pH dependent shift from −1 to +1, in particular with respect to U_{248}. However, we also observed a shift in the pH dependence for G_{248} when the structure of the N_{+1}/N_{+72} base pair was altered. Given that $A_{248(wt)}$ is in close proximity to the cleavage site[18] these data are consistent with a model where changes of the structural architecture at and near the cleavage site in the RPR-substrate complex (see above) affect the charge distribution. As a consequence, this influences the positioning of the Mg^{2+} that activates the water that acts as the nucleophile resulting in a shift of the phosphorus to be attacked[31,43]; for an alternative rational see[25].

Proposed function of the well-conserved residue $A_{248(wt)}$ in wild type RPR and base stacking to prevent unspecific hydrolysis. In the RNase P tRNA crystal structure, which represents the post-cleavage stage, $A_{248(wt)}$ stacks on top of the tRNA G_{+1}/C_{+72} base pair and presents the Hoogsteen surface facing the G_{+1} and the tRNA 5′ end (Fig. 9A)[17]; see also Refs[20,63]. The importance of the $A_{248(wt)}$ Hoogsteen surface for substrate interaction has been implicated on the basis of nucleotide analogue-modification interferences studies[32]. However, we provided data suggesting that the Hoogsteen surface of $A_{248(wt)}$ is not engaged in pairing with N_{-1}, at least not in the case of pMini3bp substrates[31]. This raises the question about the role and function of $A_{248(wt)}$. The structure of yeast $tRNA^{Phe}$ reveals that the discriminator base at position +73 stacks on top of the G_{+1}/C_{+72} pair (Fig. 9B)[64]. As such, the discriminator base acts as a hydrophobic cap that restricts access of bulk H_2O to the terminal base pair[65,66]. Binding of pre-tRNA to the RPR results in formation of the RCCA-RNase P RNA interaction where the discriminator base pairs with residue U_{294}[18,27,34]. In the RNase P-tRNA complex $A_{248(wt)}$ stacks on the G_{+1}/C_{+72} base pair by occupying the position that the discriminator base has in free tRNA (Fig. 9A,B). This contributes to anchor the substrate to the RPR[18,20,63]. In addition, we propose that the $A_{248(wt)}$ stacking on G_{+1}/C_{+72} prevents water from accessing the hydrophobic amino acid acceptor stem and potential unspecific hydrolysis of the tRNA after cleavage. We foresee that this also occurs prior to cleavage of the pre-tRNA and the recent cryoEM structures of *Eco* RNase P in complex with pre-tRNA support that this is indeed the case[63]. In this context the stacking free energy for A would be more favorable, followed by G, C and U[67]. Moreover, considering the activation energy (E_a), our findings indicated that the trend is $A_{248(wt)} < G_{248} < C_{248} < U_{248}$ with $A_{248(wt)}$ having the lowest activation energy barrier (Table 4). These data provide reasons to why $A_{248(wt)}$ in bacterial RPR is well conserved.

We also note that the E_a value for cleavage of pATSerUG with $A_{248(wt)}$ was determined to be 12 kJ/mole (Table 4), which is two- to three-fold lower than for cleavage of pre-$tRNA^{Tyr}$Su3, both with and without the RNase P protein C5[68]. This difference could depend on substrate and/or reaction conditions. In pre-$tRNA^{Tyr}$Su3 both the discriminator base (A_{+73}) and the first 3′ C (C_{+74}) pair with U_{-1} and G_{-2} in the 5′ leader, respectively, rendering A_{+73} and C_{+74} less accessible for interacting with RPR, i.e. formation of the "RCCA-RPR interaction" (see above[13]), compared to pATSerUG (Fig. 3). Also, here the experiments were performed at high Mg^{2+} and at a lower pH than in our previous study[68], which are also factors to consider.

To conclude, in addition to its contribution to anchor the substrate[18,20,63] we suggest that the function of $A_{248(wt)}$ is to replace the tRNA discriminator base and prevent access of water that would lead to unspecific hydrolysis/cleavage of the pre-tRNA in the RNase P-substrate complex. *Saccharomyces cerevisiae* RPR lacks an A at the position corresponding to *Eco* RPR $A_{248(wt)}$. Interestingly, in the cryo-EM structure of *S. cerevisiae* RNase P in complex with pre-tRNA the 5′ leader residues A_{-1} and A_{-2} stack on top of the tRNA G_{+1}/C_{+72} pair forming a hydrophobic cap[19]. According to our proposal this would also prevent unspecific hydrolysis/cleavage of the pre-tRNA. Given that POP5 amino acid residues are also positioned close to the G_{+1}/C_{+72} pair these might also contribute to prevent access of H_2O and unspecific hydrolysis/cleavage (see also below).

Prevention of unspecific hydrolysis in PRORP. Like RNase P, proteinaceous PRORPs cleave the 5′ leader of pre-tRNAs and recent data show that the N_{-1} identity also influences cleavage by PRORPs both with respect to cleavage site recognition and rate of cleavage[69–71]. The crystal structures of PRORP1 and PRORP2 are available[72,73]; for a cryo structure see[74], whereas the structure of PRORP in complex with its pre-tRNA substrate is not. Structural and mechanistic studies suggest that D474 and D475 coordinate Me(II) in the PRORP1 active site. Given the similarities between RNA and protein-based RNase P activities, i.e., the need to cleave pre-tRNAs correctly and prevent unspecific hydrolysis, it is likely that stacking on top of the N_{+1}/N_{+72} base pair is also present in the PRORP-pre-tRNA complex. Candidates to act as a hydrophobic cap during the PRORP catalyzed reaction might be aromatic amino acids such as W478 and F500, which both are positioned close to the Me(II)-ion in the active site. Another possibility is that the pre-tRNA discriminator base keeps its position and stacks on

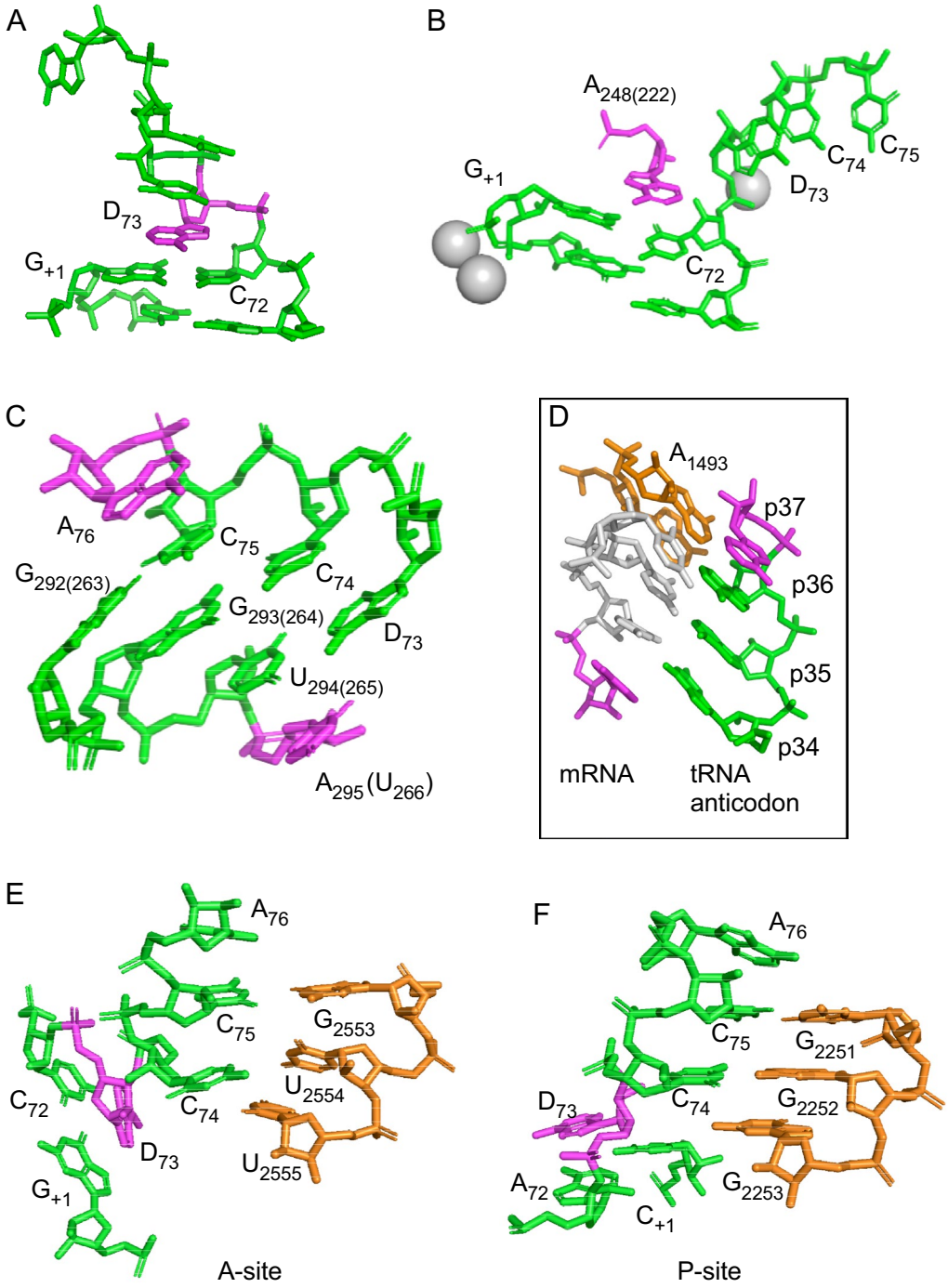

Figure 9. Illustration of base stacking. (**A**) Stacking of the discriminator base, D_{+73} (in magneta), on the G_{+1}/C_{+72} base pair in the crystal structure of $tRNA^{Phe}$ (PDB code 1EVV)[64]. (**B**) Stacking of residue A_{248} (in magenta and *E. coli* numbering, Fig. 1) on the $tRNA^{Phe}$ G_{+1}/C_{+72} base pair (in green) in the crystal structure of the RNase P-$tRNA^{Phe}$ complex (PDB code 3Q1R)[18]. Grey spheres represent Me(II)-ions. (**C**) Stacking and the RCCA-RPR interaction (in green) in the crystal structure of the RNase P-$tRNA^{Phe}$ complex (PDB code 3Q1R)[18]. Stacking residues in magenta. D_{73} corresponds to the discriminator base at position +73 in $tRNA^{94}$ while the RPR numbering refers to *E. coli* numbering (Fig. 1). Note that A_{295} in *E. coli* corresponds to U_{266} in *T. maritima* RPR[18]. Stacking residues, the tRNA 3′ terminal A_{76} and the RPR residue, are marked in magenta. (**D**) Codon-anticodon interaction in the ribosomal A-site where residues in magenta stack as shown in the figure. p34–p37 correspond to positions in the tRNA anticodon loop. Gray residues represent the codon and residues marked in orange residues correspond to A1492 and A1493 in 16S rRNA (PDB code 2J02)[80]. (**E**,**F**) Stacking interactions in the ribosomal peptidyl transfer center, panel E (A-site) and panel F (P-site) as indicated. Orange residues correspond to rRNA residues interacting with the tRNA, green residues refer to tRNA and the tRNA discriminator base is highlighted in magenta (PDB code 5IBB)[79]. The images were created using PyMOL (Schrödinger, LLC).

top of the N_{+1}/N_{+72} pair (and/or residues in the pre-tRNA 5′ leader, see above) in the PRORP-substrate complex as observed in other protein-tRNA complexes (see below). It will be interesting to determine whether this is the case and, if so, how access of water to the "inside" of the hydrophobic amino acid acceptor stem is prevented in the PRORP-substrate complex.

Base stacking and prevention of unspecific hydrolysis of RNA. Crystal structures of amino-acyl-tRNA synthetase-tRNA complexes (such as ArgRS-$tRNA_{Arg}$ and MetRS-$tRNA_{Met}$), EF-Tu-$tRNA^{Phe}$, the CCA adding enzyme in complex with a tRNA mimic and tRNA bound to the ribosome show that the discriminator base at +73 stacks on the G_{+1}/C_{+72} pair in a similar way as shown in Fig. 9A (see also E,F)[75–79]. In all these examples the discriminator is a purine. Moreover, inspection of the RCCA-RNase P RNA interaction in the RNase P-tRNA crystal structure reveals that U_{266} stacks on the A_{+73}/U_{265} base pair, while the 3′ terminal A_{+76} stacks on the C_{+75}/G_{263} base pair (Fig. 9C; note that the *T. maritima* residues G_{264}, U_{265} and U_{266} correspond to G_{292}, U_{294} and A_{295} in wild type *Eco* RPR, see Fig. 1)[18]. A similar type of stacking can also be observed in the ribosomal A- and P-sites both in the case of tRNA and mRNA interaction as well as with respect to the pairing between C_{74} and C_{75} and rRNA (Fig. 9D–F)[79–81]. Together this further emphasizes the importance of stacking. It is conceivable that a function of this "type" of base stacking is to prevent the access of water to functionally important base pairing interactions, and thereby ensuring high fidelity during RNA processing and decoding of mRNA.

Materials and methods

Preparation of substrates and RPR. The $tRNA^{Ser}$Su1 precursor (pSu1) N_{-1} variants were generated as run-off transcripts using T7 DNA-dependent RNA polymerase and PCR-amplified templates as described elsewhere[33,82]. The model hairpin loop substrate N_{-1} series (pATSer, pATSer-GAAA-tetra loop and pMini3bp) were purchased from Thermo Scientific Dharmacon, USA. The substrates were [γ-^{32}P]-ATP 5′ end-labeled and gel-purified followed by overnight Bio-Trap extraction (Schleicher and Schuell, GmbH, Germany; Elutrap in USA and Canada) and phenol–chloroform extraction as described elsewhere[15,31].

The construction of the gene encoding *Eco* RPR_{G248} was recently reported[31], while the C_{248} and U_{248} variants behind the T7 promoter were generated following the same procedure as outlined elsewhere using the wild type *Eco* $RPR_{A248(wt)}$ gene as template and appropriate oligonucleotides[12,31,83,84]. The RPRs were generated as run-off transcripts using T7 DNA-dependent RNA polymerase and PCR-amplified templates[31,82].

Structural probing of the Eco RPR variants. The *Eco* RPR variants were 3′-end labeled with [^{32}P]pCp and structurally probed using Pb^{2+} and RNase T1 under native conditions as described elsewhere[31,34,35,45,85]. Briefly, approximately 2 pmols of labeled RPR in 10 µl was pre-incubated for 10 min at 37 °C in 50 mM Tris–HCl (pH 7.5), 100 mM NH_4Cl and 10 mM $MgCl_2$ together with 4 µM of the unlabeled corresponding RPR. Cleavage was initiated by adding freshly prepared $Pb(OAc)_2$ to a final concentration of 0.5 mM and the reaction was stopped after 10 min. In the digestion with RNase T1, the RPR was pre-incubated as described above. One unit of RNase T1 was added followed by incubation on ice for 10 min. The reactions were stopped by adding two volumes of stop solution (10 M urea, 100 mM EDTA). The products were analyzed on 8% (w/v) denaturing polyacrylamide/7 M urea gels.

Cleavage assays and determination of k_{app}. The cleavage reactions were conducted in buffer C [50 mM 4-morpholineethanesulfonic acid (MES) and 0.8 M NH_4Cl (pH 6.1)] at 37 °C and 800 mM $Mg(OAc)_2$. The RPRs were pre-incubated at 37 °C in buffer C and 800 mM $Mg(OAc)_2$ for at least 10 min to allow proper folding before mixing with pre-heated (37 °C) substrate. In all the experiments the concentrations of substrates were ≤ 0.02 µM, while the concentrations of the RPR variants were as indicated in Table and Figure legends. The reactions were terminated by adding two volumes of stop solution (see above). The products were separated on 25% (w/v) polyacrylamide/7 M urea gels.

Cleavage of $pATSerU_{am}G$ derivatives at 37 °C was performed in buffer C and 800 mM $Mg(OAc)_2$ at pH 5.2, pH 6.1 and pH 7.2[39,40].

The rate constant k_{app} was determined under single-turnover condition at 800 mM Mg^{2+} in buffer C. The concentrations of *Eco* RPR variants used to generate the data are specified in the respective Table legends. The concentrations of pSu1 (precursor-$tRNA^{Ser}$Su1[34]) and model substrates[15,31,34] were ≤ 0.02 µM (see also the main text). For rate calculations, we used the 5′ cleavage fragment as a measure of product formed. In each assay, the time of incubation was adjusted to ensure that the velocity measurements were in the linear range (typically ≤ 10%, but never exceeding that 40% of the substrate had been consumed). Each k_{app} value is reported as a mean ± deviation of this value, which was calculated using data (six time points) from at least three independent experiments.

Determination of the kinetic constants k_{obs}, k_{obs}/K^{sto} and K^{sto}. The rate constants k_{obs} and k_{obs}/K^{sto} were determined under saturating single-turnover conditions at pH 6.1 (where cleavage is suggested to be rate limiting) and 800 mM Mg^{2+} using pATSerUG, as described elsewhere, e.g.[37]. Under these conditions we have argued elsewhere that $K^{sto} \approx K_d$ in the *Eco* RPR-alone reaction[12,30,31,86,87]. The final concentrations of the different RPR variants were between 0.8 and 6.4 µM; the concentration of the pATSerUG substrate was ≤ 0.02 µM. To ensure that the experiments were done under single-turnover conditions, the lowest concentration of RPR was > 10 times higher than the concentration of the substrate. For the calculations we used the 5′ cleavage fragment, and the time of cleavage was adjusted to ensure that the velocity measurements were in the linear range (see above). To be able to compare with our previously published data, k_{obs} and k_{obs}/K^{sto} were obtained by linear regression from Eadie-Hofstee plots as described elsewhere[12,30,31,37,88,89]. Each value is an average of at least three independent experiments and is given as a mean ± the deviation of this value.

Data availability

The datasets used are available from the corresponding author.

Received: 23 February 2023; Accepted: 23 August 2023
Published online: 29 August 2023

References

1. Guerrier-Takada, C., Gardiner, K., Marsh, T., Pace, N. & Altman, S. The RNA moiety of ribonuclease P is the catalytic subunit of the enzyme. *Cell* **35**, 849–857 (1983).
2. Liu, F. & Altman, S. R. *Protein Reviews* Vol. 10 (Springer, 2010).
3. Holzmann, J. *et al.* RNase P without RNA: Identification and functional reconstitution of the human mitochondrial tRNA processing enzyme. *Cell* **135**, 462–474 (2008).
4. Gobert, A. *et al.* A singel arabidopsis organellar protein has RNase P activity. *Nat. Struct. Mol. Biol.* **17**, 740–744 (2010).
5. Lai, L. B. *et al.* A functional RNase P protein subunit of bacterial origin in some eukaryotes. *Mol. Genet. Genomics* **286**, 359–369 (2011).
6. Taschner, A. *et al.* Nuclear RNase P of Trypanosoma brucei: A single protein in place of the multicomponents RNA-protein complex. *Cell Rep.* **2**, 19–25 (2012).
7. Nickel, A. I., Wäber, N. B., Gößringer, Lechner, M., Linne, U., Toth, U., Rossmanith, W. & Hartmann, R.K. Minimal and RNA-free RNase P in Aquifex aeolicus. *Proc. Natl. Acad. Sci. USA* **114**, 11121–11126 (2017).
8. Pannucci, J. A., Haas, E. S., Hall, T. A., Harris, J. K. & Brown, J. W. RNase P RNAs from some archaea are catalytically active. *Proc. Natl. Acad. Sci. USA* **96**, 7803–7808 (1999).
9. Tsai, H.-Y., Pulukkunat, D. K., Woznick, W. K. & Gopalan, V. Functional reconstitution and characterization of Pyrococcus furiosus RNase P. *Proc. Natl. Acad. Sci. USA* **103**, 16147–16152 (2006).
10. Kikovska, E., Svärd, S. G. & Kirsebom, L. A. Eukaryotic RNase P RNA mediates cleavage in the absence of protein. *Proc. Natl. Acad. Sci. USA* **104**, 2062–2067 (2007).
11. Lai, L. B., Vioque, A., Kirsebom, L. A. & Gopalan, V. Unexpected diversity of RNase P, an ancient tRNA processing enzyme: Challenges and prospects. *FEBS Lett.* **584**, 287–296 (2010).
12. Sinapah, S. *et al.* Cleavage of model substrates by archaeal RNase P: Role of protein cofactors in cleavage-site selection. *Nucleic Acids Res.* **39**, 1105–1116 (2011).
13. Kirsebom, L. A. & Svärd, S. G. Base pairing between *Escherichia coli* RNase P RNA and its substrate. *EMBO J.* **13**, 4870–4876 (1994).
14. Loria, A. & Pan, T. Recognition of the T stem-loop of a pre-tRNA substrate by the ribozyme from *Bacillus subtilis* ribonuclease P. *Biochemistry* **36**, 6317–6325 (1997).
15. Brännvall, M., Kikovska, E., Wu, S. & Kirsebom, L. A. Evidence for induced fit in bacterial RNase P RNA-mediated cleavage. *J. Mol. Biol.* **372**, 1149–1164 (2007).
16. Kirsebom, L. A. RNase P RNA mediated cleavage: substrate recognition and catalysis. *Biochimie* **89**, 1183–1194 (2007).
17. Kirsebom, L. A. & Trobro, S. RNase P RNA-mediated cleavage. *IUBMB Life* **61**, 189–200 (2009).
18. Reiter, N. J. *et al.* Structure of a bacterial ribonuclease P holoenzyme in complex with tRNA. *Nature* **468**, 784–789 (2010).
19. Lan, P., Tan, M., Zhang, Y., Niu, S. et al. Structural insight into precursor tRNA processing by yeast ribonuclease P. *Science* **362**, eaat6678 (2018).
20. Wan, F. *et al.* Cryo-electron microscopy structure of an archaeal ribonuclease P holoenzyme. *Nat. Commun.* **10**, 2617 (2019).
21. Wu, J. *et al.* Cryo-EM structure of the human ribonuclease P holoenzyme. *Cell* **175**, 1393–1404 (2018).
22. Phan, H.-D., Lai, L. B., Zahurancik, W. J. & Gopalan, V. The many faces of RNA-based RNase P, an RNA-world relic. *TIBS* **46**, 976–991 (2021).
23. Leontis, N. B. & Westhof, E. Conserved geometrical base-pairing patterns in RNA. *Q. Rev. Biophys.* **31**, 399–455 (1998).
24. Zahler, N. H., Christian, E. L. & Harris, M. E. Recognition of the 5′ leader of pre-tRNA substrates by the active site of ribonuclease P. *RNA* **9**, 734–745 (2003).
25. Zahler, N. H., Sun, L., Christian, E. L. & Harris, M. E. The pre-tRNA nucleotide base and 2′-hydroxyl at N(-1) contribute to fidelity in tRNA processing by RNase P. *J. Mol. Biol.* **345**, 969–985 (2005).
26. Kufel, J. & Kirsebom, L. A. Different cleavage sites are aligned differently in the active site of M1 RNA, the catalytic subunit of *Escherichia coli* RNase P. *Proc. Natl. Acad. Sci. USA* **93**, 6085–6090 (1996).
27. Brännvall, M., Pettersson, B. M. F. & Kirsebom, L. A. Importance of the +73/294 interaction in *Escherichia coli* RNase P RNA substrate complexes for cleavage and metal ion coordination. *J. Mol. Biol.* **325**, 697–709 (2003).
28. Behra, P. R. K., Pettersson, B. M. F., Das, S., Dasgupta, S. & Kirsebom, L. A. Comparative genomics of *Mycobacterium mucogenicum* and *Mycobacterium neoaurum* clade members emphasizing tRNA and non-coding RNA. *BMC Evol. Biol.* **19**, 124 (2019).
29. Brännvall, M. & Kirsebom, L. A. Complexity in orchestration of chemical groups near different cleavage sites in RNase P RNA mediated cleavage. *J. Mol. Biol.* **351**, 251–257 (2005).
30. Wu, S., Kikovska, E., Lindell, M. & Kirsebom, L. A. Cleavage mediated by the catalytic domain of bacterial RNase P RNA. *J. Mol. Biol.* **422**, 204–214 (2012).
31. Wu, S. *et al.* Transition-state stabilization in *Escherichia coli* ribonuclease P RNA-mediated cleavage of model substrates. *Nucleic Acids Res.* **42**, 631–642 (2014).
32. Siew, D., Zahler, N. H., Cassano, A. G., Strobel, S. A. & Harris, M. E. Identification of adenosine functional groups involved in substrate binding by the ribonuclease P ribozyme. *Biochemistry* **38**, 873–1883 (1999).
33. Kirsebom, L. A. & Svärd, S. G. Identification of a region within M1 RNA of *Escherichia coli* RNase P important for the location of the cleavage site on a wild-type tRNA precursor. *J. Mol. Biol.* **231**, 594–604 (1993).
34. Kufel, J. & Kirsebom, L. A. The P15-loop of Escherichia coli RNase P RNA is an autonomous divalent metal ion binding domain. *RNA* **4**, 777–788 (1998).
35. Brännvall, M. & Kirsebom, L. A. Metal ion cooperativity in ribozyme cleavage of RNA. *Proc. Natl. Acad. Sci. USA* **98**, 12943–12947 (2001).
36. Brännvall, M. & Kirsebom, L. A. Manganese ions induce miscleavage in the *Escherichia coli* RNase P RNA-catalyzed reaction. *J. Mol. Biol.* **292**, 53–63 (1999).
37. Wu, S., Chen, Y., Lindell, M., Mao, G. & Kirsebom, L. A. Functional coupling between a distal interaction and the cleavage site in bacterial RNase P RNA-mediated cleavage. *J. Mol. Biol.* **411**, 384–396 (2011).
38. Persson, T., Cuzic, S. & Hartmann, R. K. Catalysis by RNase P RNA: unique features and unprecedented active site plasticity. *J. Biol. Chem.* **278**, 43394–43401 (2003).
39. Brännvall, M., Kikovska, E. & Kirsebom, L. A. Cross talk between the +73/294 interaction and the cleavage site in RNase P RNA mediated cleavage. *Nucleic Acids Res.* **32**, 5418–5429 (2004).
40. Kikovska, E., Brännvall, M. & Kirsebom, L. A. The exocyclic amine at the RNase P cleavage site contributes to substrate binding and catalysis. *J. Mol. Biol.* **359**, 572–584 (2006).

41. Niranjanakumari, S., Stams, T., Crary. S. M., Christianson, D. W. & Fierke, C. A. Protein component of the ribozyme ribonuclease P alters substrate recognition by directly contacting precursor tRNA. *Proc. Natl. Acad. Sci. USA* **95**, 15212–15217 (1998).
42. Jovanovic, M., Sanchez, R., Altman, S. & Gopalan, V. Elucidation of structure-function relationships in the protein subunit of bacterial RNase P using a genetic complementation approach. *Nucleic Acids Res.* **30**, 5065–5073 (2002).
43. Kirsebom, L. A. Roles of metal ions in RNase P catalysis. In Liu, F., Altman, S (eds), Protein Reviews Vol 10: Ribonuclease P. Springer Science+Business Media, LLC, 233 Springer Street, New York, NY, 10013, USA pp 113–134 (2010).
44. Mao, G., Srivastava, A. S., Kosek, D., Lindell, M. & Kirsebom, L. A. Critical domain interactions for type A RNase P RNA-mediated catalysis with and without the specificity domain. *PLoS ONE* **13**, e0192873 (2018).
45. Kufel, J. & Kirsebom, L. A. Residues in *Escherichia coli* RNase P RNA important for cleavage site selection and divalent metal ion binding. *J. Mol. Biol.* **263**, 685–698 (1996).
46. Loria, A. & Pan, T. Recognition of the 5′ leader and the acceptor stem of a pre-tRNA substrate by the ribozyme from *Bacillus subtilis* RNase P. *Biochemistry* **37**, 10126–10133 (1998).
47. Burgin, A. B. & Pace, N. R. Mapping the active site of ribonuclease P RNA using a substrate containing a photoaffinity agent. *EMBO J.* **9**, 4111–4118 (1990).
48. Haas, E. S., Brown, J. W., Pitulle, C. & Pace, N. R. Further perspective on the catalytic core and secondary structure of ribonuclease P RNA. *Proc. Natl. Acad. Sci. USA* **91**, 2527–2531 (1994).
49. Schlegl, J., Hardt, W.-D., Erdmann, V. A. & Hartmann, R. K. Contribution of structural elements to *Thermus thermophilus* ribonuclease P RNA function. *EMBO J.* **13**, 4863–4869 (1994).
50. Brown, J. W. *et al.* Comparative analysis of ribonuclease P RNA using gene sequences from natural microbial population reveals tertiary structural elements. *Proc. Natl. Acad. Sci. USA* **93**, 3001–3006 (1996).
51. Pomeranz-Krummel, D. A. & Altman, S. Verification of phylogenetic predictions in vivo and the importance of the tetraloop motif in a catalytic RNA. *Proc. Natl. Acad. Sci. USA* **96**, 11200–11205 (1999).
52. Baird, N. J., Fang, X. W., Srividya, N., Pan, T. & Sosnick, T. R. Folding of a universal ribozyme: the ribonuclease P RNA. *Q. Rev. Biophys.* **40**, 113–161 (2007).
53. Perreault, J. P. & Altman, S. Important 2′-hydroxyl groups in model substrates for M1 RNA, the catalytic RNA subunit of RNase P from *Escherichia coli*. *J. Mol. Biol.* **226**, 399–409 (1992).
54. Perreault, J. P. & Altman, S. Pathway of activation by magnesium ions of substrates for the catalytic subunit of RNase P from *Escherichia coli*. *J. Mol. Biol.* **230**, 750–756 (1993).
55. Forster, A. C. & Altman, S. External guide sequences for an RNA enzyme. *Science* **249**, 783–786 (1990).
56. Smith, D. & Pace, N. R. Multiple magnesium ions in the ribonuclease P reaction mechanism. *Biochemistry* **32**, 5273–5281 (1993).
57. Brown, R. S., Dewan, J. C. & Klug, A. Crystallographic and biochemical investigation of the lead(II)-catalyzed hydrolysis of yeast phenylalanine tRNA. *Biochemistry* **24**, 4785–4801 (1985).
58. Behlen, L. S., Sampson, J. R., DiRenzo, A. B. & Uhlenbeck, O. C. Lead-catalyzed cleavage of yeast tRNAPhe mutants. *Biochemistry* **29**, 2515–2523 (1990).
59. Tallsjö, A., Svärd, S. G., Kufel, J. & Kirsebom, L. A. A novel tertiary interaction in M1 RNA, the catalytic subunit of *Escherichia coli* RNase P. *Nucleic Acids Res.* **21**, 3927–3933 (1993).
60. Kikovska, E., Mikkelsen, N.-E. & Kirsebom, L. A. The naturally trans-acting ribozyme RNase P RNA has leadzyme properties. *Nucleic Acids Res.* **33**, 6920–6930 (2005).
61. Miller, P. S., Bhan, P. & Kan L-S. Synthesis and interactions of oligodeoxyribonucleotides containing 2′-amino-2′-deoxyuridine. *Nucleosides Nucleotides* **12**, 785–792 (1993).
62. Aurup, H., Tuschl, T., Benseler, F., Ludwig, J. & Eckstein, F. Oligonucleotide duplexes containing 2′-amino-2′-deoxycytidines: Thermal stability and chemical reactivity. *Nucleic Acids Res.* **22**, 20–24 (1994).
63. Zhu, J. *et al.* Structural and mechanistic basis for recognition of alternative tRNA precursor substrates by bacterial ribonuclease P. *Nat. Commun.* **13**, 5120 (2022).
64. Jovine, L., Djordjevic, S. & Rhodes, D. The crystal structure of yeast phenylalanine tRNA at 2.0 Å resolution: cleavage by Mg(2+) in 15-year old crystals. *J. Mol. Biol.* **301**, 401–414 (2000).
65. Maltseva, T. V., Agback, P. & Chattopadhyaya, J. How much hydration is necessary for the stabilisation of DNA-duplex?. *Nucleic Acids Res.* **21**, 4246–4252 (1993).
66. Isaksson, J. & Chattopadhyaya, J. A uniform mechanism correlating dangling-end stabilization and stacking geometry. *Biochemistry* **44**, 5390–5401 (2005).
67. Saenger, W. *Principles of nucleic acid structure* (Springer-Verlag, 1984).
68. Tallsjö, A. & Kirsebom, L. A. Product release is a rate-limiting step during cleavage by the catalytic RNA subunit of *Escherichia coli* RNase P. *Nucleic Acids Res.* **21**, 51–57 (1993).
69. Brillante, N. *et al.* Substrate recognition and cleavage-site selection by a single-subunit protein-only RNase P. *Nucleic Acids Res.* **44**, 2323–2336 (2016).
70. Howard, M. J. *et al.* Differential substrate recognition by isozymes of plant protein-only ribonuclease P. *RNA* **22**, 782–792 (2016).
71. Mao, G. *et al.* Cleavage of model substrates by *Arabidopsis thaliana* PRORP1 reveals new insights into its substrate requirements. *PLoS ONE* **11**, e0160246 (2016).
72. Howard, M. J., Lim, W. H., Fierke, C. A. & Koutmos, M. Mitochondrial ribonuclease P structure provides insight into the evolution of catalytic strategies for precursor-tRNA 5′ processing. *Proc. Natl. Acad. Sci. USA* **109**, 16149–16154 (2012).
73. Karasik, A., Shanmuganathan, A., Howard, M. J., Fierke, C. A. & Koutmos, M. Nuclear protein-only ribonuclease P2 structure and biochemical characterization provide insight into the conserved properties of tRNA 5′ end processing enzymes. *J. Mol. Biol.* **428**, 26–40 (2016).
74. Feyh, R., Waeber, N. B., Prinz, S., Giammarinaro, P. I., Bange, G., Hochberg, G., Hartmann, R. K. & Altegoer, F. Structure and mechanistic features of the prokaryotic minimal RNase P. *eLife* **10**, e70160 (2021).
75. Nissen, P., Kjeldgaard, M., Thirup. S., Polekhina, G., Reshetnikova, L., Clark, B. F. S. & Nyborg, J. Crystal structure of the ternary complex of Phe-tRNAPhe, EF-Tu and a GTP analog. *Science* **270**, 1464–1472 (1995).
76. Nakanishi, K., Ogiso, Y., Nakama, T., Fukai, S. & Nureki, O. Structural basis for anticodon recognition by methionyl-tRNA synthetase. *Nat. Struct. Mol. Biol.* **12**, 931–932 (2005).
77. Konno, M. *et al.* Modeling of tRNA-assisted mechanism of Arg activation based on a structure of Arg-tRNA synthetase, tRNA, and an ATP analog (ANP). *FEBS J.* **276**, 4763–4779 (2009).
78. Pan, B., Xiong, Y. & Steitz, T. A. How the CCA-adding enzyme selects adenine of cytosine at position 76 of tRNA. *Science* **330**, 937–940 (2010).
79. Rozov, A., Westhof, E., Yusupov, M. & Yusupova, G. The ribosome prohibits the G.U wobble geometry at the first position of the codon-anticodon helix. *Nucleic Acids Res.* **44**, 6434–6441 (2016).
80. Selmer, M., Dunham, C. M., Murphy IV, F. V., Weixlbaumer, A, Petry, S., Kelley, A. C., Weir, J. R. & Ramakrishnan, V. Structure of the 70S ribosome complexed with mRNA and tRNA. *Science* **313**, 1935–1942 (2006).
81. Satpati, P., Sund, J. & Åqvist, J. Structure-based energetics of mRNA decoding on the ribosome. *Biochemistry* **53**, 1714–1722 (2014).
82. Milligan, J. F., Groebe, D. R., Witherell, G. W. & Uhlenbeck, O. C. Oligoribonucleotide synthesis using T7 RNA polymerase and synthetic DNA templates. *Nucleic Acids Res.* **15**, 8783–8798 (1987).

83. Vioque, A., Arnez, J. & Altman, S. Protein-RNA interactions in the RNase P holoenzyme from *Escherichia coli*. *J. Mol. Biol.* **202**, 835–848 (1988).
84. Kikovska, E., Wu, S., Mao, G. & Kirsebom, L. A. Cleavage mediated by the P15 domain of bacterial RNase P RNA. *Nucleic Acids Res.* **40**, 2224–2233 (2012).
85. Ciesiolka, J., Hardt, W. D., Schlegl, J., Erdmann, V. A. & Hartmann, R. K. Lead-ion-induced cleavage of RNase P RNA. *Eur. J. Biochem.* **219**, 49–56 (1994).
86. Stage-Zimmermann, T. K. & Uhlenbeck, O. C. Hammerhead ribozymes kinetics. *RNA* **4**, 875–889 (1998).
87. Chen, W.-Y., Pulukkunat, D. K., Cho, I.-M., Tsai, H.-Y. & Gopalan, V. Dissecting functional cooperation among protein subunits in archaeal RNase P, a catalytic ribonucleoprotein complex. *Nucleic Acids Res.* **38**, 8316–8327 (2010).
88. Hofstee, B. H. J. On the evaluation of the constants Vm and Km in enzyme reactions. *Science* **116**, 329–331 (1952).
89. Dowd, J. E. & Riggs, D. S. A comparison of estimates of Michaelis-Menten kinetic constants from various linear transformation. *J. Biol. Chem.* **240**, 863–869 (1965).
90. Massire, C., Jaeger, L. & Westhof, E. Derivation of the three-dimensional architecture of bacterial ribonuclease P RNAs from comparative sequence analysis. *J. Mol. Biol.* **279**, 773–793 (1998).
91. Brännvall, M., Mikkelsen, N.-E. & Kirsebom, L. A. Monitoring the structure of *Escherichia coli* RNase P RNA in the presence of various divalent metal ions. *Nucleic Acids Res.* **29**, 1426–1432 (2001).
92. Guerrier-Takada, C. & Altman, S. Structure in solution of M1 RNA, the catalytic subunit of ribonuclease P from *Escherichia coli*. *Biochemistry* **23**, 6327–6334 (1984).
93. Torres-Larios, A., Swinger, K. K., Krasilnikov, A. S., Pan, T. & Mondragón, A. Crystal structure of the RNA component of bacterial ribonuclease P. *Nature* **437**, 584–587 (2005).
94. Crothers, D. M., Seno, T. & Söll, D. Is there a discriminator site in transfer RNA. *Proc. Natl. Acad. Sci. USA* **69**, 3063–3067 (1972).

Acknowledgements

We thank our colleagues for discussions throughout this work and with respect to stacking special thanks to Dr J. Chattopadhyaya. Dr SG Svärd, Dr AC Forster and Ms T Bergfors for critically reading the manuscript.

Author contributions

L.A.K. conceived the study. G.M., A.S.S., S.W. and D.K. performed the experiments and assisted in preparing the Figs. 1, 2, 3, 4, 5, 6, 7 and 8. L.A.K., G.M., A.S.S., S.W. and D.K. analyzed and interpreted the data. L.A.K. and G.M. wrote the manuscript. All authors read and approved the final version of the manuscript.

Funding

Open access funding provided by Uppsala University. This work was funded by the Swedish Research Council (N/T), the Uppsala RNA Research Center (Swedish Research Council Linneus support) and Carl Tryggers Foundation to LAK. Funding for open access charge: Uppsala University.

Competing interests

The authors declare no competing interests.

Additional information

Correspondence and requests for materials should be addressed to L.A.K.

Reprints and permissions information is available at www.nature.com/reprints.

Publisher's note Springer Nature remains neutral with regard to jurisdictional claims in published maps and institutional affiliations.